Preclinical Study of Cannflavins A and B Action Against Glioblastoma Cells

Jennifer Holborn [a], Hannah Robeson [a,1], Ellis Chartley [a,1], Tiana Gluscevic [a,b,1], Adina Borenstein [a], Colby Perrin [a], Begüm Alural [a], Himain Perera [a], Tariq A. Akhtar [a], Nina Jones [a], Jasmin Lalonde [a,*]

[a] Department of Molecular and Cellular Biology, University of Guelph, 50 Stone Road E, Guelph, ON N1G 2W1, Canada

[b] Canurta Therapeutics, 2425 Matheson Blvd. E, Suite 807, Mississauga, ON, L4W 5K4, Canada

[1] These authors contributed equally to this study.

* Corresponding author: **Jasmin Lalonde**

Email address: jlalon07@uoguelph.ca

Phone: (519) 824-4120 x. 54706

ORCID: 0000-0002-6797-1894 (J. Lalonde)

Keywords: Cannflavins, Cerebral organoids, Flavonoids, Glioblastoma multiform, Invasion, Migration

22 *Abbreviations:* AKT, Protein kinase B; BDNF, Brain-Derived Neurotrophic Factor; BSA,
23 Bovine Serum Albumin; DMEM, Dulbecco's Modified Eagle's Medium; DMSO,
24 Dimethylsulfoxide; FBS, Fetal Bovine Serum; GBM, Glioblastoma multiform; GFP,
25 Green Fluorescent Protein; iPSC, induced Pluripotent Stem Cell; MAPK, Mitogen-
26 Activated Protein Kinase; mTOR, mammalian target of rapamycin; NF-κB, Nuclear factor-
27 κB; PBS, Phosphate Buffered Saline; RTK, Receptor Tyrosine Kinase; TMZ,
28 Temozolomide; TrkB, Tropomyosin receptor kinase B.

ABSTRACT (250 WORDS)

Background: Flavonoids represent a large group of naturally occurring polyphenolic compounds, many of which have been found to produce valuable biological outcomes, including action against cancer cells. Glioblastoma multiforme (GBM) is an aggressive type of brain tumor that is associated with a poor prognosis and has limited treatment options. Previous findings suggest that cannflavins can produce promising effects for pancreatic and bladder cancers, but the efficacy of these phytochemicals in attacking brain tumour cells remains unknown. Our study evaluates the potential of cannflavin A and cannflavin B against GBM cells using a range of *in vitro* approaches.

Results: We conducted experiments using A-172 and U-87 GBM lines to assess the impact of cannflavins A and B on cell viability, cycle, migration, and invasion capacity. Our results revealed a consistent dose-dependent decrease in cell viability in both lines after the addition of cannflavin B to the culture media. Interestingly, we found that chrysoeriol (the non-prenylated synthesis precursor of cannflavins in the *Cannabis sativa* plant) only has a limited adverse effect on survival using the same approach, while techtochrysin (an O-methylated flavone) has none. Using time-lapse live-cell imaging and a scratch assay, we also show that cannflavins can inhibit tumor cell migration at concentrations below those that produce significant cell death. Finally, we found that cannflavin B exhibits anti-migratory and anti-invasive properties in transwell and tumorsphere assays, underscoring its multifaceted therapeutic potential.

Conclusion: These findings suggest that cannflavin B holds promise as a therapeutic agent in the treatment of GBM.

51 **HIGHLIGHTS (3-5 BULLET POINTS)**

52 • Cannflavin B but not cannflavin A limits the viability of A-172 and U-87 GBM cells
53 in a concentration- and time-dependent manner.
54 • Using time-lapse live-cell imaging and a scratch assay, we provide evidence that
55 cannflavins A and B can inhibit GBM cell migration at concentrations below those
56 that result in a significant reduction in cell viability.
57 • Cannflavin B exhibits robust anti-migratory and anti-invasive properties in transwell
58 and tumorsphere assays, underscoring its multifaceted therapeutic potential.
59 • Although previous work had reported the capacity of cannflavins A and B to interfere
60 with TrkB and downstream the MAPK/AKT signaling pathways in mouse primary
61 neurons, the effect of those molecules is limited in GBMs, suggesting that other targets
62 are engaged to produce the cellular effects.
63

64 **INTRODUCTION**

65 Flavonoids are naturally occurring polyphenolic molecules that accumulate in dietary items
66 such as fruits, vegetables, and teas. This broad group of phytochemicals has received
67 considerable research attention for over 25 years due to their beneficial anti-inflammatory
68 and anti-oxidative properties (Panche *et al.*, 2016). Many flavonoids have also attracted
69 interest in cancer research due to their potential therapeutic applications. For instance,
70 kaempferol has been found to induce G2/M cell cycle arrest as well as reduce migration
71 and invasion in breast, liver, ovarian, lung, and brain cancers (Gao et al., 2018; Jo et al.,
72 2015; Li et al., 2017; Zhu et al., 2019). Apigenin and luteolin, for their part, have shown
73 promise as anti-cancer agents for breast, prostate, lung, and brain subtypes by suppressing
74 the mitogen-activated protein kinase (MAPK) and Protein kinase B (AKT) signaling
75 pathways that control cell proliferation and survival (Cheng et al., 2013; Erdogan et al.,
76 2016; Huang et al., 2019; Tseng et al., 2017). Finally, quercetin, one of the most consumed
77 dietary flavonoids, induces G2/M phase arrest and significantly increases tumor suppressor
78 protein p53 expression in MDA-MB-453 breast cancer cells (Choi et al., 2008). It also
79 limits angiogenesis and metastasis of other cancer cell types through changes in
80 MAPK/AKT/mTOR signaling pathways (Balakrishnan et al., 2016; Gao et al., 2012; Kim
81 et al., 2019; Lee et al., 2015; Pratheeshkumar et al., 2012). Taken together, these examples
82 support searching for additional flavonoids that also produce robust anti-cancer effects.

83 Cannflavins are prenylated and highly lipophilic metabolites first purified 40 years ago
84 from *Cannabis sativa (C. sativa)* plant extracts (Barrett et al., 1985). As illustrated in
85 **Supplementary Figure 1**, the cannflavin family includes five known members, which are
86 cannflavin A, cannflavin B, cannflavin C, isocannflavin B (also known as FBL-03G), and

87 8-prenylcannflavin B (also known as dorsmanin D). Several of these molecules have been
88 shown to produce promising effects applicable to various clinical conditions. For instance,
89 studies revealed the anti-inflammatory properties of cannflavins A and B through their
90 ability to inhibit pro-inflammatory mediators and the production of prostaglandin E_2 at a
91 rate thirty times more potent than aspirin (Barrett et al., 1985; Werz et al., 2014). Consistent
92 with their anti-inflammatory activity, Eggers and colleagues (2019) have reported
93 neuroprotective action of cannflavin A in neuronal PC12 cells against amyloid β-induced
94 cell death by reducing $A\beta_1$-42 aggregation and fibril formation. In the setting of cancer,
95 research suggests that certain cannflavins produce desirable effects under specific
96 circumstances. For instance, isocannflavin B was found to improve survival in preclinical
97 mouse models of metastatic pancreatic cancer by increasing apoptosis of tumor cells
98 (Moreau et al., 2019), and cannflavin A has been reported to synergize with agents
99 commonly used to treat bladder cancer at specific concentrations (Tomko et al., 2022).
100 Despite those promising results, whether cannflavins can effectively attack brain cancer
101 cells has not been directly studied.

102 Glioblastoma multiforme (GBM) is the most aggressive and common primary brain
103 tumor in adults, characterized by rapid growth and diffuse infiltration into surrounding
104 healthy brain tissues (Tilak et al., 2021a). The prognosis for GBM patients is extremely
105 poor, with a median survival of approximately 15 months despite aggressive treatment
106 (Johnson and O'Neill, 2012; Ostrom et al., 2020). The standard of care for GBM is
107 maximum safe surgical resection followed by a combination of radiation therapy and
108 temozolomide (TMZ) chemotherapy, a DNA alkylating agent that induces cell death
109 through DNA lesions (Stupp et al., 2005; Stupp et al., 2009; Fisher and Adamson, 2021).

110 However, the inability to fully resect the tumor with surgery, combined with the persistence
111 of TMZ-resistant cancer cells capable of recapitulating tumors, typically leads to disease
112 relapse within just a few months (Weller et al., 2013; Birzu et al., 2020). Therefore, there
113 is a pressing need to identify new agents that could improve patient prognosis.

114 In this study, we conducted experiments using A-172 and U-87 GBM lines to measure
115 the effects of cannflavins A and B on cell viability, migration, and invasion capacity. Our
116 work revealed an apparent decrease in GBM cell viability following exposure to increasing
117 concentrations of cannflavin B. Additionally, analysis of cell migration using a time-lapse
118 live-cell scratch assay revealed the potential of cannflavins to impede tumor dissemination
119 at concentrations below those inducing cell death. Specifically, cannflavin B exhibited
120 robust anti-migratory and anti-invasive properties, as evidenced by transwell and
121 tumorsphere invasion assays, highlighting its multifaceted therapeutic effects. Finally, as
122 our previous work found interference of TrkB signaling by cannflavin A and cannflavin B
123 in mouse primary neurons (Holborn et al., 2023), we also evaluated whether the action of
124 cannflavins on GBM cells could be tied to reduced activity of this receptor tyrosine kinase
125 (RTK). Together, our findings underscore the promising anti-cancer properties of
126 cannflavin B against immortalized GBM cells, suggesting its potential role as a novel
127 therapeutic agent.

128 **MATERIALS AND METHODS**

129 *Cell culture and reagents*

130 Malignant male glioma cell lines A-172 and U-87 MG (U-87) were obtained from the
131 American Type Culture Collection (ATCC, USA, Cat No. CRL-1620 and HTB-14,
132 respectively). Cells were cultured in DMEM (Gibco, USA, Cat No. 11965-092)
133 supplemented with 10% FBS (Gibco, Cat No. 12483-020) and 0.5%
134 penicillin/streptomycin (Gibco, Cat No. 155140-122), at 37°C and 5% CO_2. For treatment
135 with cannflavins and other tested agents, the molecules were dissolved in DMSO and
136 applied directly to the culture media.

137 The BIONi010-A cell line (European Bank for induced Pluripotent Stem Cells,
138 ECACC Cat No. 66540022) used to prepare cerebral organoids was purchased from Sigma-
139 Aldrich (St-Louis, MO, USA) and cultured in ExCellerate iPSC Expansion Medium (R&D
140 Systems, Cat No. CCM036) according to the manufacturer's instructions.

141

142 *Antibodies and pharmacological compounds*

143 The antibodies recognizing phosphorylated p44/p42 MAPK (Cat No. 4370), AKT (Cat No.
144 4691), phosphorylated AKT Thr 308 (AKT T308, Cat No. 2965), and phosphorylated AKT
145 Ser 473 (AKT S473, Cat No. 4060) were acquired from Cell Signaling Technology
146 (Beverly, MA, USA). The antibody detecting phosphorylated TrkB Tyr705 (TrkB Y705,
147 Cat No. ab229908) was from Abcam (Waltham, MA, USA), the antibody recognizing p42
148 MAPK (Erk2, sc-1647) was from Santa Cruz Biotechnology (Santa Cruz, CA), the
149 GAPDH (Cat No. AB2302) antibody was from Sigma-Aldrich, and the Tubulin β 3 (TUJ1,
150 Cat No. 801202) antibody was from BioLegend (San Diego, CA, USA). Finally, the GFP

151 (Cat No. 10262) and cross-absorbed secondary antibodies (horseradish peroxidase- and
152 fluorophore-conjugated) were from Invitrogen.

153 Cannflavin A (Cat No. C-291001) and cannflavin B (Cat No. C-291003) were
154 purchased from TLC Pharmaceutical Standards (Newmarket, ON, Canada). ANA-12 (Cat
155 No. SML0209) was acquired from Sigma-Aldrich, and chrysoeriol (Cat No. 491-71-4)
156 from Cayman Chemical (Ann Arbor, MI, USA).

157 Techtochrysin was biosynthesized as follows: The *O. basilicum* O-methyl transferase
158 ObFOMT1 (Accession number JQ653275) open reading frame was synthesized by Twist
159 Bioscience (San Francisco, CA, USA) in the *pET28a* vector system between the *NdeL* and
160 *XhoI* sites. This system inserted an N-terminal hexahistidine tag into the coding sequence.
161 The construct was then introduced into *E. coli* BL21-CodonPlus (DE3)-RIPL. Bacterial
162 cells harboring the expression vector were cultured in LB media at 37°C to an OD_{600} of
163 0.6. Isopropyl-β-D-thiogalactoside was added to a final concentration of 0.2 mM, and
164 cultures were further incubated at 16°C for an additional 16 hours to allow for protein
165 expression. Thereafter, *E. coli* cells were collected by centrifugation, resuspended in Buffer
166 A (20 mM Tris-HCl, 500 mM KCl, pH 8.0) and lysed using an Emulsiflex. Cell debris and
167 remaining intact cells were removed from the solution by centrifugation (20,000 x *g*, 20
168 minutes at 4°C) and the supernatant was applied to a 1 mL HisTrap FF column (Cytiva,
169 Marlborough, MA) equilibrated in Buffer B (20 mM Tris-HCl, 500 mM KCl, 20 mM
170 imidazole, pH 8.0). Proteins bound to the Ni^{2+} affinity matrix were washed with fifteen
171 column volumes of Buffer B, eluted with one column volume of Buffer C (20 mM Tris-
172 HCl, 500 mM KCl, 200 mM imidazole, pH 8.0), and then immediately desalted on PD-10
173 columns (Cytiva) equilibrated with Buffer D (50 mM Tris-HCl, 5 mM $MgCl_2$, pH 8.0, 10%

174 glycerol). The concentration of recombinant ObFOMT1 was determined by Bradford
175 Assay using BSA as a standard, and 1 mg was used per enzymatic assay to produce
176 techtochrysin. Precisely, purified recombinant ObFOMT1 was mixed in 10 mL of assay
177 solution (1 mM chrysin, 10% w/v hydroxypropyl-β-cyclodextrin, 2 mM S-
178 adenosylmethionine, and 5 mM $MgCl_2$ in 50 mM Tris-HCl, pH 8.0) and incubated with
179 shaking for 16 hours at 15°C. Reagents for the assay solution were obtained from Xi'an B-
180 Thriving I/E Co., Ltd (Xi'an, Shaanxi, China). The enzymatic reaction was terminated by
181 adding 1 mL of 10% formic acid. Prenylated bibenzyl products were extracted with three
182 volumes of ethyl acetate three times, evaporated to dryness with gaseous N, and
183 resuspended in 6 mL of methanol. The sample was chromatographed on an Infinity Lab
184 Poroshell 120 EC-C18 2.7 µM (ODS2 9.4 x 150 mm) column and resolved by an Agilent
185 1260 infinity HPLC using a linear gradient with solvent A (45% methanol, 0.1% formic
186 acid in water) and solvent B (95% methanol, 0.1% formic acid in water) at a flow rate of
187 2.5 mL/min heated at 30°C. The gradient started at 60% of solvent B and increased to 70%
188 in 7 minutes, then increased to 100% of solvent B in 1 minute and remained isocratic for 2
189 minutes. Techtochrysin was detected by absorption at 340 nm and was collected from the
190 HPLC at 9.3 minutes. Finally, the eluate was dried under gaseous nitrogen, lyophilized,
191 and techtochrysin quantified relative to a standard curve generated with chrysin. Product
192 identity was confirmed based on mass spectral fragmentation patterns.
193
194 *Cell viability assay*
195 Cell viability was assessed using a resazurin reduction assay, as described previously
196 (Holborn et al., 2023). Briefly, A-172 and U-87 cells were seeded in 96 multi-well plates

197 at a density of 1.0 x 10^4 per well and allowed to attach overnight. Cells were then treated
198 with DMSO and varying concentrations of ANA-12 (1 to 50 μM) or cannflavins (1 to 20
199 μM) diluted in Opti-MEM reduced serum media (Gibco, Cat No. 31985070) and incubated
200 at 37°C for the indicated time. Following treatment, resazurin sodium salt (Sigma-Aldrich,
201 Cat No. R7017) was dissolved in Hank's balanced salt solution (Wisent Inc., Saint-Jean-
202 Baptiste, QC, Canada, Cat No. 311-513-CL), diluted 1:10 in each well, and cells were
203 further incubated at 37°C for three hours. Fluorescence was measured on a microplate
204 reader at 570/590 nm, and a background control was subtracted from each value. All
205 treatments were completed in triplicate.

206 The following procedure was used for quantification: First, fluorescence values were
207 exported from the microplate reader, and the average of three background control wells
208 with Opti-MEM reduced serum media only was subtracted from each treatment value.
209 Second, the subtracted values were multiplied by 100 and divided by the average of the
210 DMSO controls to obtain a percentage relative to the vehicle control. Finally, the average
211 of three replicates per treatment was used as the final value for one biological replicate. A
212 minimum of three biological replicates were taken.

213

214 *Lactate dehydrogenase cytotoxicity assay*

215 Lactate dehydrogenase (LDH) release was measured using the CyQUANT LDH
216 Cytotoxicity Assay Kit according to the manufacturer's protocol (Invitrogen, Cat No.
217 C20300). Briefly, A-172 and U-87 cells were seeded in 96-well multiplates and treated
218 with the tested molecules, using a similar approach to the resazurin reduction assay. Before
219 the treatment endpoint, 10× Lysis Buffer was applied to control wells for 10 minutes to get

220 the Maximum LDH Release value. Cell culture supernatant from each treatment was
221 transferred to a new 96-well multiplate, an equal volume of reaction mixture was added,
222 mixed, and then the plate was incubated at room temperature for 30 minutes, protected
223 from light. Absorbance was measured on a microplate reader at 490 nm and 680 nm
224 (background). All treatments were completed in triplicate.

225 The following procedure was used for quantification: First, LDH activity was
226 calculated by subtracting the raw absorbance value measured at 680 nm from the 490 nm
227 value for each replicate and treatment. The average of three background control wells with
228 Opti-MEM reduced serum media was subtracted from each treatment value. Finally, the
229 LDH activity of each technical replicate of the compound-treated wells was divided by the
230 average of the maximum LDH activity and multiplied by 100 to obtain the percent
231 cytotoxicity. The average of the triplicates per treatment was taken and used as the final
232 value for one biological replicate; three biological replicates were completed in total.

233

234 *Terminal deoxynucleotidyl transferase dUTP nick end labeling (TUNEL) assay*

235 The Roche *in Situ* Cell Death Detection Kit, Fluorescein (Sigma-Aldrich, Cat No.
236 11684795910), was used according to the manufacturer's protocol. Briefly, A-172 cells
237 were fixed using 4% paraformaldehyde for 15 minutes after treatment, then incubated for
238 2 minutes in permeabilization solution (0.1% Triton X-100, 0.1% sodium citrate in PBS).
239 This was followed by a 1-hour incubation in the dark at 37°C with humidity in TUNEL
240 reaction solution. After rinsing with PBS three times for 10 minutes, cells were incubated
241 in 4',6-diamidino-2-phenylindole (DAPI; Invitrogen, Cat No. 62247) staining solution for

242 10 minutes and finally washed in PBS twice for 10 minutes before being mounted onto
243 slides with ProLong Diamond Antifade (Invitrogen, Cat No. P36930).
244
245 *Flow cytometry*
246 A-172 cells and U-87 cells were seeded in 6-well plates at a density of 2.5 x 10^5 per well
247 and allowed to attach overnight. The next day, cells were treated with DMSO control,
248 cannflavin A, or cannflavin B (1 and 5 μM) for 24 hours. Following that time, the cell
249 monolayer was dissociated with trypsin, pelleted, resuspended in FACS buffer (PBS
250 supplemented with 2% FBS and 1 mM EDTA), and frozen fixed at -20°C in 70% ethanol.
251 Immediately before running samples, fixed cells were thawed and washed twice in FACS
252 buffer, 50 μL of 100 μg/mL RNAse A (Thermo Fisher Scientific, Cat No. EN0531) in
253 FACS buffer was added for 30 minutes, then 200 μL of 0.25 μg/mL propidium iodide
254 (Molecular Probes, Cat No. P-1304) in FACS buffer was added for 10 minutes in the dark.
255 The DNA contents were analyzed using a Northern Lights cytometer (Cytek Biosciences,
256 Bethesda, MD, USA).
257 Data quantification was performed using FlowJo v10.10 software. First, debris was
258 excluded using SSC-A vs. FSC-A gating strategy, and then singlets were selected using
259 FSC-H vs. FSC-A. Specifically, the univariate cell cycle platform Watson Pragmatic
260 algorithm distributed cell cycle peaks to the histograms presented, and data points were
261 plotted as a percentage of the cell count found in each cell cycle phase (G1, S, G2/M).

262 *Transwell invasion assay*

263 The bottoms of Corning Transwell inserts (New York, USA, Cat No. CLS3442) were
264 coated with 20 µg/mL fibronectin (Sigma-Aldrich, Cat No. F1141-1MG) at 4°C for 1 hour.
265 After three washes with PBS, the tops were coated with 0.2 mg/mL Corning Matrigel
266 matrix (Cat No. 354234) overnight at 37°C. In parallel with the preparation of the
267 transwells, A-172 cells were seeded at a density of 1.5 x 10^5 cells per well in 6-well plates
268 and grown to 85-90% confluency for 24 hours. They were then treated overnight with 10
269 µM cannflavin B or DMSO in DMEM containing 1% FBS media. The next day, 30,000
270 live cells from each condition were collected and seeded in the upper chamber of each well
271 with DMEM containing 1% FBS plus cannflavin B (10 µM), and in the bottom chamber
272 with DMEM containing 10% FBS. Cells were allowed to invade the Matrigel matrix for
273 24 hours at 37°C and 5% CO_2. Afterward, the transwell membranes containing the invaded
274 cells were removed. The membranes were stained with a 1% crystal violet solution in 20%
275 methanol for 20 minutes, washed three times with PBS, and dried for several hours at room
276 temperature. Representative photographic images of the membranes were taken and then
277 cut out. Finally, crystal violet was eluted from each membrane with 10% acetic acid for 20
278 minutes, and the absorbance (at 562 nm) of the eluates was measured to quantify invasion.
279 Three biological replicates with each treatment run in duplicate were analyzed.

280

281 *Scratch migration assay*

282 A-172 cells were seeded in a 6-well plate at a density of 2.0 x 10^5 per well and grown to
283 complete confluency in DMEM supplemented with 10% FBS for 48 hours. Using a P1000
284 pipette tip, 4 crossing linear wounds were created through the monolayer of cells within

285 each well. Next, the unattached cells were washed away with PBS before being added back
286 to culture media supplemented with DMSO only or the treatment molecules. Baseline
287 images of the wound area were acquired immediately after adding the culture media using
288 a phase-contrast inverted Nikon Eclipse Ti2-E microscope (Nikon Instruments, Melville,
289 NY, USA) equipped with a motorized stage and STXF stage top incubator (Tokai Hit USA
290 Inc., PA, USA) to maintain temperature (37°C), humidity, and CO_2 (5%, 150 mL/min)
291 constant. Two separate areas per scratch were imaged every 15 minutes over a 48-hour
292 period. NIS-Elements Advanced Research software was used to run binary area fraction
293 analysis, and the number of migrated cells was counted using ImageJ v1.54 software. Three
294 biological replicates were performed for each treatment condition.
295
296 *Generation of tumorspheres (tumor spheroids)*
297 The tumorsphere protocol was adapted from previous work (Vinci et al., 2015; Tilak et al.,
298 2021b). Briefly, U-87 cells were passaged at least three times in complete media and then
299 20,000 cells per well were seeded into a clear round-bottom ultra-low attachment
300 microplate (Corning, Cat No. 7007). Tumorspheres were allowed to form for 5 days at
301 37°C and 5% CO_2, with half the media changed on Day 3.
302
303 *Tumorsphere invasion assay*
304 Individual tumorspheres prepared as mentioned above were embedded in Corning Matrigel
305 matrix (Cat No. 354234) containing the specified treatment. Four tumorspheres with a
306 circular shape and no protrusions were chosen per treatment, and half the media was
307 removed from the well. An equal volume of Matrigel supplemented with treatment at 2x

308 concentration was added to each well and incubated at 37°C and 5% CO_2 for one hour to
309 polymerize. Treatments at 1x of the desired treatment concentration were prepared in
310 complete media and added to each well immediately after incubation. The plate was then
311 imaged on a Nikon Eclipse Ti2-E inverted microscope equipped with a motorized stage,
312 image stitching capability, and a 10× objective at 0, 24, 48, and 72 hours. One image per
313 tumorsphere per treatment (4 tumorspheres and 4 treatments for 16 images at each time
314 point) was analyzed, and three biological replicates were performed.

315 The image analysis on original tiff files was performed with ImageJ as follows: For
316 the area measurement, the elliptical tool was used to encircle each tumorsphere, ensuring
317 all cells grown out from the original tumorsphere were included in the area measurement.
318 Three area measurements were taken for each tumorsphere at each time point and averaged.
319 For the radius measurement, the line tool was used to measure from the center point of the
320 tumorsphere out to the furthest protrusion from the tumorsphere. Three radius
321 measurements were taken for each tumorsphere at each time point and averaged. The
322 average area or radius of each treatment was divided by the DMSO control average at its
323 corresponding time point to obtain the values used for statistical analysis.

324

325 *Generation of cerebral organoids*

326 BIONi010-A induced pluripotent stem cells (iPSCs) were cultured on Matrigel-coated
327 plates (Corning, Cat No. 354277) in ExCellerate iPSC Expansion Medium (R&D Systems,
328 Cat No. CCM036). Cerebral organoids were generated using the STEMdiff Cerebral
329 Organoid Kit (StemCell Technologies, Cat No. 08570) as described in the manufacturer's
330 protocol and Tilak and colleagues (2021b). Briefly, on Day 0, iPSCs were lifted with

331 Gentle Cell Dissociation Reagent, resuspended in embryoid body (EB) Seeding Medium,
332 and seeded in an ultra-low attachment, round bottom 96-well plate (Corning, Cat No. 7007)
333 at a density of 9,000 cells/well. EB Formation Medium was added on Days 2 and 4, and
334 on Day 5, EBs were transferred to ultra-low attachment 24-well plates (Corning, Cat No.
335 3473) containing Induction Medium for 48 hours. On Day 7, EBs were encased in droplets
336 of Matrigel on organoid embedding sheets (StemCell Technologies, Cat No. 08579), which
337 were allowed to polymerize at 37°C before being washed into ultra-low attachment 6-well
338 plates (Corning, Cat No. 3471) using 3 mL of Expansion Medium. On Day 10, the
339 Expansion Medium was replaced with Maturation Medium, and the plate was transferred
340 to an orbital shaker inside a 37°C, 5% CO_2 incubator. The media was changed three times
341 per week until Day 60, the beginning of the organoid co-culture assay.
342
343 *Organoid co-culture assay*
344 The organoid co-culture assay protocol was modified from Tilak and colleagues (2021b).
345 Tumorspheres were generated similar to above, except with 12,000 GFP-expressing U-87
346 cells seeded per well. Sixty (60)-day-old organoids were removed from the 6-well plate
347 and placed individually in 1.5 mL Eppendorf tubes, each containing 4 tumorspheres and
348 500 μL of Maturation Medium. Tubes were incubated at 37°C and 5% CO_2 inside 10 cm
349 dishes with the caps open to allow airflow during attachment, while maintaining a sterile
350 environment. After 48 hours, 50% of the media was replaced, and after 72 hours, organoids
351 with tumorsphere attached were gently removed from the tubes using a wide-bore pipette
352 and put back in 6-well plates on the orbital shaker for an additional 24 hours (for the 10-
353 day experiment) or 8 days (for the 3-day experiment), at which point cannflavin B (5 μM)

354 or DMSO was added to the well in a complete media change. Media containing cannflavin
355 B or DMSO was replaced every other day for the duration of the experiment. Fourteen days
356 after initiating the co-culture, all organoids were removed from the wells, washed three
357 times with PBS, and fixed in 4% paraformaldehyde overnight at 4°C. Organoids were
358 washed again with PBS and incubated in a 30% sucrose solution at 4°C for 4 days before
359 being embedded in a 7.5% gelatin, 10% sucrose solution and snap-frozen in dry ice
360 submerged in 95% ethanol. Twenty (20) µm sections were obtained using a cryostat (Leica,
361 CM1860), placed on Vectabond-coated slides (Vector Laboratories, Cat No. SP-1800-7),
362 and stored at -80°C until immunostaining.

363 For immunostaining, organoid sections were washed 3 times with PBS and blocked in
364 10% normal goat serum in PBS at room temperature for 30 minutes. Sections were
365 incubated overnight at 4°C in blocking solution containing primary antibodies (TUJ1 and
366 GFP, 1:1,000). Slides were washed again 3 times with PBS and incubated in Alexa Fluor-
367 488- or Alexa Fluor-594-conjugated secondary antibodies (Invitrogen, Cat Nos. A11039
368 and A11032) in 5% normal goat serum in PBS for 2 hours at room temperature. Slides
369 were washed 3 additional times in PBS, counterstained with DAPI, and cover-slipped with
370 ProLong Glass Antifade mounting reagent (Invitrogen, Cat No. P36984).

371 Captures were taken using a Nikon Eclipse Ti2-E microscope at 20× magnification.
372 Exposure for each channel was kept consistent between conditions. For analyzing
373 tumorsphere area, a section from approximately the middle of each tumorsphere to be
374 analyzed was immunostained, and the perimeter of the GFP signal was traced using the
375 polygon selection tool in ImageJ software by an individual blinded to the experimental
376 conditions.

377 *Western blotting*

378 For western blot analysis, cells were seeded in 6-well plates and grown for 2 to 3 days
379 before treatment. After treatment, cells were collected with radioimmunoprecipitation
380 assay (RIPA) buffer (50 mM Tris [pH 8.0], 0.5% Igepal-CA-630, 0.1% SDS, 0.5%
381 deoxycholic acid, 1 mM EDTA, 300 mM NaCl), supplemented with Phosphatase Inhibitor
382 Cocktail 3 (Sigma-Aldrich, Cat No. P0044) and EDTA-free Protease Inhibitor Cocktail
383 (Sigma-Aldrich, Cat No. 11836170001), and homogenized using QIAshredder columns
384 (QIAGEN, Cat No. 79656). Concentration of all lysates was measured using Pierce BCA
385 Assay Kit (Thermo Fisher Scientific, Cat No. 23225), one volume of 2× Laemmli buffer
386 (100 mM tris-HCl [pH 6.8], 4% SDS, 0.15% bromophenol blue, 20% glycerol, 200 mM β-
387 mercaptoethanol) was added, samples were adjusted to an equal concentration, and finally
388 boiled for 5 minutes. A total of 15 μg of protein was run on a 10% SDS-PAGE gel and
389 transferred to a nitrocellulose membrane. Membranes were incubated in TBST (Tris-
390 buffered saline and 0.1% Tween 20) supplemented with 5% non-fat powdered milk for 30
391 min at room temperature, and then probed overnight with the intended primary antibody at
392 the following dilution: P-TrkB Y705 (1:1,000), P-AKT S473 (1:1,000), P-AKT T308
393 (1:1,000), pan-AKT (1:2,000), P-p44/p42 MAPK (1:1,000), p42 MAPK (1:1,000), and
394 GAPDH (1:20,000). The next day, membranes were washed with TBST, incubated with
395 the appropriate secondary antibody, and visualized using enhanced chemiluminescence
396 (ECL), according to the manufacturer's guidelines (Pierce, Thermo Fisher Scientific). Each
397 experiment was repeated three times.

398 The western blots were quantified as follows: First, equal amount of protein sample
399 was analyzed by SDS-PAGE for each biological replicate. Second, the exposure time of

400 the film to ECL was the same for each biological replicate. Third, the exposed films were
401 scanned using a HP LaserJet Pro M377dw scanner in grayscale at a resolution of 300 dpi.
402 Finally, protein expression was quantified using ImageJ software to determine the mean
403 grey value of the protein bands, with the background value subtracted. The pixel density
404 for all data was inverted by subtracting the mean grey value from 255. The final values of
405 each protein band were taken as a ratio over the corresponding loading control to provide
406 a normalized value for statistical analysis.
407

408 *Statistical analysis*

409 All statistical calculations were completed with Prism 10 (GraphPad Software, Boston,
410 MA, USA). No statistical methods were employed to predetermine the sample size of any
411 of the presented experiments. Student *t*-test or analysis of variance (ANOVA) plus Tukey's
412 post hoc test for multiple comparisons was performed where indicated. A value of $p \leq .05$
413 was considered statistically significant. No test for outliers was conducted, and no data
414 point was excluded. Unless mentioned otherwise, all results represent the mean ± SEM
415 from at least three independent experiments ($n = 3$). Sample size was determined based on
416 previous studies of a similar nature (Lalonde et al., 2021; Holborn et al., 2023; Lau et al.,
417 2025).
418

419 **RESULTS**

420 *Cannflavin B decreases GBM cell viability*

421 The flavonol kaempferol and flavone apigenin have been shown to significantly reduce the
422 viability of different cancer cell types in the low micromolar concentration range after 24-

423 48 hours of exposure (e.g., Gao *et al.*, 2018; Tseng *et al.*, 2017). Except for the work of
424 Moreau and colleagues (2019) with mouse models of metastatic pancreatic cancer and the
425 study by Tomko and colleagues (2022) that reported a promising effect of cannflavin A
426 against bladder carcinoma cells, we know little about the impact of cannflavins on other
427 cancer types. This prompted us to thoroughly test the effect of cannflavin A and cannflavin
428 B on the viability of the A-172 and U-87 GBM cell lines. Importantly, we used the small-
429 molecule non-competitive TrkB antagonist ANA-12 (Cazorla et al., 2011) as a comparison
430 compound for this analysis because it has been reported to reduce the viability of A-172
431 cells in a dose- and time-dependent manner (Pinheiro et al., 2017). Hence, this represents
432 a relevant reference measure that also connects with our recent publication demonstrating
433 the interference of cannflavins A and B on TrkB signaling in mouse primary cortical
434 neurons (Holborn et al., 2023).

435 As presented in **Figure 1**, applying cannflavin A and cannflavin B in the 1-20 μM
436 final concentration range to the culture media of either A-172 (**Fig. 1A-C**) and U-87 (**Fig.**
437 **1D-F**) cells produced similar mixed results. Specifically, no significant effect on viability
438 was detected using a resazurin reduction assay for cannflavin A at any concentration or
439 time-point, although a trend for reduced viability can be observed in A-172 cells with the
440 highest concentration (20 μM) at the 24-hour and 48-hour time-points. On the other hand,
441 cannflavin B produced a robust reduction in viability for both A-172 and U-87 cells, with
442 the most significant effect observed at higher concentrations (20 μM) and longer treatment
443 times (48 hours). Interestingly, ANA-12 in the 20-50 μM range also negatively affected
444 survival in both cell lines, with the notable difference that higher compound concentrations
445 were required to achieve an impact comparable to that of cannflavin B. This can be best

446 appreciated at 48 hours in A-172 cells, where 5 μM cannflavin B reduced viability below
447 50%, while ANA-12 at 10 μM had no statistically significant effect (estimated average cell
448 viability of 90%). Together, these results establish that cannflavin B is more potent in
449 affecting the survival of GBM cells than cannflavin A and ANA-12.

450 To gain a broader view of the potency of cannflavin B towards U-87 cells, we next
451 performed a similar experiment with two structurally related flavones, namely chrysoeriol,
452 the non-prenylated synthesis precursor of cannflavins in the *C. sativa* plant (**Fig. S2A**, Rea
453 et al., 2019), and techtochrysin (**Fig. S2B**), an O-methylated flavone previously discovered
454 to have effects against SW480 and HCT116 colon cancer cells through inhibition of
455 Nuclear factor-κB (NF-κB) activity (Park et al., 2015). Interestingly, we found that the
456 direct application of chrysoeriol to the cell culture medium significantly reduced the
457 viability of U-87 cells, but only at a final concentration of 20 μM and treatment times of
458 24-48 hours (**Fig. S2C**). This result suggests that the prenyl group found at the 3' position
459 of the flavone B-ring that distinguishes cannflavin B from chrysoeriol contributes to the
460 potency of the latter molecule in this assay. The effect of techtochrysin, however, opposed
461 that of chrysoeriol. Intriguingly, application of techtochrysin in the range of 5-40 μM for
462 24-48 hours significantly enhanced the viability of U-87 cells. In summary, these
463 experiments reinforce the notion that cannflavin B produces anti-survival effects on GBM
464 cells at a lower concentration and faster than closely related flavones.

465 *Cannflavins A and B do not induce necrosis in GBM cells*

466 To assess the extent to which cannflavin B's observed impact on GBM cell viability could
467 be attributed to necrosis, we performed cell membrane integrity tests with the lactate
468 dehydrogenase (LDH) release assay. A-172 and U-87 cells treated with 10-20 μM

469 cannflavin A or cannflavin B for 24 hours presented minimal LDH release (**Fig. S3A, B**).
470 Specifically, application of cannflavin A resulted in 3.57% LDH release at 10 μM and
471 2.54% at 20 μM in A-172 cells, and 0.96% at 10 μM and 1.03% at 20 μM in U-87 cells.
472 For cannflavin B, LDH release was 4.43% at 10 μM and 5.38% at 20 μM in A-172 cells,
473 and 0.81% at 10 μM and 0.88% at 20 μM in U-87 cells. Those values are comparable to
474 those obtained with ANA-12 at a concentration of 10 μM (2.01% for A-172 cells and
475 1.61% for U-87). In summary, these results suggest that the adverse effect of cannflavin B
476 on cell viability, as assessed using the resazurin reduction method, is not due to necrotic
477 cell death at the specified concentrations and time points.
478
479 *Cannflavins A and B do not cause apoptosis in the low micromolar range*
480 Our following goals were to assess the effect of cannflavins A and B in the low micromolar
481 range on GBM's cell cycle, migration, and capacity to invade. Before proceeding with
482 those tests, though, we wanted to confirm that neither cannflavin A nor cannflavin B causes
483 widespread programmed cell death resulting in DNA fragmentation after at least 24 hours
484 of exposure to the compound. Using the highly sensitive TUNEL assay, we observed that
485 A-172 GBM cells treated with cannflavin A or cannflavin B at a final concentration of 10
486 μM for 24 hours did not produce a noticeable fluorescein signal indicative of apoptosis
487 (**Fig. S3C**). This negative result assures that any effect associated with cannflavins at a
488 concentration of 10 μM or lower, which will be identified next, is distinct from
489 programmed cell death.

490 *Effect of cannflavins on A-172 and U-87 cell cycle*

491 Various flavonoids have been demonstrated to affect the cell cycle of different cancer cell
492 types (e.g., Lin et al., 2015; Srivastava et al., 2016; Zhang et al., 2017). This led us to ask
493 whether cannflavins A and B, at concentrations that do not produce a rapid and significant
494 anti-viability effect on A-172 and U-87 cells, could alter their cell cycle. Flow cytometry
495 analysis showed that neither cannflavin A nor cannflavin B affected cell cycle phase after
496 24 hours of treatment in the concentration range of 1-5 μM (**Fig. 2**). Interestingly, the A-
497 172 and U-87 cell lines exhibited distinctive distributions of the cell cycle that remained
498 unchanged with treatment (G1 proportion for the DMSO control was 61.7% and 41.6%,
499 respectively). In both GBM cell lines, compared to the DMSO control, there was no
500 statistically significant change in the cell cycle phase upon cannflavin A or cannflavin B
501 treatment. These results demonstrate that cannflavins in the low micromolar range do not
502 alter GBM cell cycle.

503

504 *Cannflavins limit GBM cell migration and invasion*

505 Invasion and metastasis are primarily responsible for mortality associated with solid tumors
506 (Li et al., 2025). This is the case for GBM, where rapid invasion and damaging infiltration
507 of the cancer cells into surrounding healthy brain tissue account for most of the poor
508 outcomes (Barbaro et al., 2022). Therefore, systematically assessing the action of
509 cannflavins on GBM cell migration and invasion is highly relevant.

510 To start, we completed an analysis of cell migration using a time-lapse scratch assay
511 in which cannflavin A (10 μM final concentration), cannflavin B (5 μM final
512 concentration), ANA-12 (10 μM final concentration), or DMSO alone was applied directly

513 to the culture media of A-172 cells. Cell migration into the scratch wound area was
514 monitored over 48 hours (**Fig. 3A** and **Supplementary Video**). Our data revealed striking
515 differences in wells treated with cannflavins compared to the DMSO control. First, analysis
516 of the binary area fraction over all time-points suggested a delayed wound closure in
517 inhibitor-treated conditions and more linear cell movement over time for the DMSO and
518 cannflavin A conditions compared to the cannflavin B and ANA-12 (**Fig. 3B**). Examining
519 next just the 24-hour and 48-hour time-points, we found that the normalized wound area
520 fraction was significantly lower for the three tested molecules compared to DMSO (**Fig.**
521 **3C**). Further, considering the data as a percentage of wound closure, significantly less area
522 was covered by cells after 24 hours and 48 hours exposure to cannflavin B, but only at 48
523 hours for cannflavin A (**Fig. 3D**). ANA-12 results in that analysis were not different
524 compared to DMSO. Finally, considering the number of individual cells detectable within
525 the wound area, significantly fewer were present at the end of the experiment for cannflavin
526 B (**Fig. 3E**).

527 Next, we performed a transwell assay to gauge the potential of cannflavin B to limit
528 A-172's capacity to invade when the cells are exposed to the molecule. A-172 cells were
529 pre-treated overnight (~16 hours) with 10 μM cannflavin B or DMSO and then plated on
530 Matrigel-coated inserts with the addition of fresh cannflavin B (10 μM). As presented in
531 **Figure 4**, the results from the transwell invasion assay revealed that exposure to cannflavin
532 B significantly reduced the number of cells that invaded through the Matrigel matrix,
533 resulting in a statistically significant reduction of more than 50% compared to the vehicle
534 control. This result supports that cannflavin B at a concentration of 10 μM effectively

535 inhibits GBM cell migration and invasion, providing initial evidence of its potential against
536 tumor progression.

537 Lastly, since U-87 cells have a strong tendency to aggregate and form tumor-like
538 spheroid formations (tumorspheres) in suspension culture, we leverage this attribute to
539 provide a different evaluation of the action of cannflavins A and B on the invasion ability
540 of these GBM cell subtypes. Specifically, we cultured U-87 as 3-dimensional (3D)
541 tumorspheres and then embedded those within a Matrigel matrix to measure how they
542 would progress in the outward direction (**Fig. 5A**). Interestingly, adding cannflavin A to
543 the culture media at a final concentration of 10 μM resulted in a significantly smaller radius
544 and area of tumorsphere outgrowth at the three examined times (**Fig. 5B, C**). For cannflavin
545 B, tumorspheres in wells treated at a final concentration of 5 μM presented a significantly
546 reduced area at 72 hours after the start of the experiment (**Fig. 5B**) and a smaller radius in
547 the 48-72 hours times (**Fig. 5C**). ANA-12, for its part, was minimally active in this assay
548 producing only a slight significant effect on radius at 72 hours (**Fig. 5C**). Taken together,
549 these three experiments provide strong evidence that cannflavins, particularly cannflavin
550 B, can produce rapid and sustained anti-migration and anti-invasion action against GBM
551 cells.

552

553 *Cannflavin B limits the growth and infiltration of U-87 GBM tumorspheres attached to*
554 *cerebral organoids*

555 Conventional pre-clinical studies for GBM consist of monolayer tumor cell cultures and
556 animal approaches, including xenografts and genetically engineered mouse models
557 (Gómez-Oliva et al., 2021; Haddad et al., 2021). However, these strategies encounter

558 significant obstacles in recapitulating the complexity of GBM, especially the variety of
559 tumor cellular states and the cancerous mass microenvironment. The use of brain organoids
560 derived from human pluripotent stem cells helps overcome some of those challenges and
561 provides exciting new ways to study GBM tumor formation and invasion in real time
562 (Linkous et al., 2019; Wang et al., 2023)—an approach that our group has used with
563 success in recent years (Tilak et al., 2021b; Lau et al., 2025). To test if cannflavin B could
564 produce therapeutically relevant effects in a more complex *in vitro* system, we conducted
565 a co-culture experiment where iPSC-derived cerebral organoids matured for 60 days were
566 mixed with U-87 tumorspheres expressing GFP (**Fig. 6A**). Our pool of co-culture
567 specimens was then divided in two groups: one where the U-87 tumorspheres attached and
568 grew unchallenged for 11 days followed by the application of cannflavin B at a final
569 concentration of 5 μM in the culture media for 3 days (Paradigm 1), and another (Paradigm
570 2) where the cancer cells attached and grew for 4 days and then 5 μM cannflavin B was
571 added for 10 days (**Fig. 6B**). Co-cultures treated with DMSO only were included for both
572 tests as control, and media change with fresh cannflavin B (5 μM) or DMSO was done
573 every other day for the duration of the experiment. As seen in fluorescence microscopy
574 captures of immunostained sections (**Figure 6C-F**), U-87 tumorspheres attached to
575 cerebral organoids with both paradigms. In the two DMSO control conditions (**Fig. 6C, E**),
576 a distinct intermingling between GBM cells expressing GFP and neurons, as revealed by
577 TUJ1 immunostaining, can be observed at the edge of the cerebral organoid where the
578 tumorsphere is attached. Interestingly, less penetration of GBM cells into the organoid
579 appeared to occur in the cannflavin B-treated wells of both tests (**Fig. 6D, F**). Finally,
580 although the tumorsphere total area for corresponding sections was not statistically

581 different between the two conditions in the 3-day (Paradigm 1) experiment (**Fig. 6G**), we
582 found that the U-87 tumorspheres were significantly smaller when cannflavin B was added
583 for 10 days (Paradigm 2, **Fig. 6H**). Together, these observations collected with a more
584 physiologically relevant model provide compelling additional data to support an effect of
585 cannflavin B against the ability of aggressive GBM cells to invade human brain-like tissue.
586

587 *Cannflavins A and B impact on TrkB signaling in GBM cells*

588 As mentioned previously, a study by Pinheiro and colleagues (2017) reported that the TrkB
589 inhibitor ANA-12 reduces the viability of A-172 cells, suggesting that the activity of this
590 RTK may be essential for the growth and survival of this GBM cell line. Since our previous
591 work using mouse primary cortical neurons also found that cannflavins A and B can
592 interfere with TrkB signaling (Holborn et al., 2023), we considered it necessary to gain
593 more information about the effect of cannflavins and ANA-12 on TrkB signaling in A-172
594 (**Fig. 7**) and U-87 (**Fig. 8**) cells to interpret our functional data. As expected, western blot
595 analysis revealed that application of cannflavin A at a final concentration of 20 μM (**Fig.**
596 **7A, B**) and cannflavin B at 10-20 μM (**Fig. 7F, G**) to the culture media of A-172 cells for
597 6 hours significantly reduced the phosphorylation of TrkB at tyrosine 705 (Y705), which
598 is in the catalytic domain and stimulates kinase activity of the receptor when
599 phosphorylated. Consistent with this result, ANA-12 at a final concentration of 10 μM also
600 significantly decreased phospho-TrkB Y705 signal (**Fig. 7B, G**). Interestingly, however,
601 our western blot data also revealed two unexpected and critical results. Firstly, key
602 downstream TrkB signaling effectors (i.e., p44/p42 MAPK and AKT) were unaffected by
603 cannflavins and ANA-12 in A-172 cells (**Fig. 7C-E, H-J**). Secondly, cannflavins and

604 ANA-12 did not impair TrkB phosphorylation and downstream signaling effectors in U-
605 87 cells, even at the highest tested concentration (**Fig. 8**). Together, these extensive western
606 blot data force the critical conclusion that any positive results about GBM survival,
607 migration, and invasion presented above are most likely distinct from TrkB signaling
608 impairment, whether they were the result of cannflavins or ANA-12 treatment.
609

610 **DISCUSSION**

611 In this study, we employed various *in vitro* assays to characterize the action of cannflavins
612 A and B on the viability, cycle, migration, and invasion capacities of A-172 and U-87 GBM
613 cells. Our results present a consistent dose-dependent decrease in cell viability for both
614 lines after applying cannflavin B to the culture media. No effect on cell cycle by either
615 cannflavin molecule was detected, but we found that both molecules can reliably limit
616 tumor cell migration below the 10 μM concentration and that cannflavin B has robust anti-
617 invasive properties based on results from transwell and tumorsphere assays. Together,
618 these observations underscore the multifaceted therapeutic potential of cannflavin B
619 against this aggressive type of brain cancer.

620 In addition, we conducted an extensive western blot analysis to gain insights about the
621 possible molecular signaling changes induced by cannflavins that could produce the
622 reported cellular effects. However, even though the tested cannflavins and ANA-12
623 consistently reduced TrkB phosphorylation at the Y705 catalytic residue in A-172 cells,
624 this effect is not observed in U-87 cells. Most importantly, cannflavins and ANA-12 had
625 minimal effects on MAPK and AKT, which are well-known contributing factors to cancer
626 hallmarks, including growth, apoptosis, and invasion. This unexpected result departs from

627 our previous work on cannflavins A and B in mouse primary cortical neurons (Holborn et
628 al., 2023) and suggests that different molecular events, influenced by cannflavins, are
629 responsible for the migration and invasion disruptions observed in GBM cells in this study.
630 Therefore, future work is needed to elucidate the target engagement of cannflavins in GBM
631 cells. One strategy for this task could be to utilize the Proteome Integral Solubility
632 Alteration (PISA) assay, a high-throughput and mass-spectrometry-based approach that
633 leverages binding-dependent changes in protein solubility to identify drug-target
634 interactions (Gaetani et al., 2019; Gaetani and Zubarev, 2023).

635 On a separate note, an intriguing finding in our study concerns the increased viability
636 of U-87 cells exposed to techtochrysin (**Fig. S2B, D**)—a flavone molecule that had been
637 reported to suppress the growth of SW480 and HCT116 human colon cancer cells by
638 inhibiting NF-κB resulting in the expression of death receptors like DR3, DR4, and Fas
639 (Park et al., 2015). Although we cannot explain at this point why U-87 cells exposed to this
640 specific flavone produced an opposite effect to what has been reported with human colon
641 cancer cells, this bring to our attention the possibility that some of the anti-cancer
642 phenotypes associated with cannflavins A and B that we found may be linked to disruption
643 of the transcription factor NF-κB. Indeed, extensive research has implicated NF-κB in
644 various aspects of cancer formation, growth, treatment response, immune escape, and other
645 related processes (Taniguchi and Karin, 2018; Zhang et al., 2021; Khan et al., 2024). In
646 GBM and other gliomas, it has been reported for more than two decades that the aberrant
647 constitutive activity of this transcription factor contributes to disease initiation and
648 progression, including the invasion phenotype (Nagaai et al., 2002; Raychaudhuri et al.,
649 2004; Wang et al., 2004). Considering this, one tantalizing scenario is the disruption by

650 cannflavins of the constitutive signaling pathway that phosphorylates and promotes
651 degradation of IκBα by the ubiquitin-proteasome system, ultimately releasing NF-κB
652 dimers that translocate to the nucleus and modulate target gene expression that contributes
653 to disease progression (Cahill et al., 2016). If this is the case, it would be revealing to test
654 the effect of cannflavin B administration in xenograft or induced mouse models of GBM
655 as used in previous work focusing on targeting aberrant NF-κB activity (Friedmann-
656 Morvinski et al., 2016). Ultimately, this would provide a direct test of this hypothesis and
657 additional pre-clinical evidence to promote cannflavin B as a potentially valuable
658 therapeutic agent against GBM.

659 Lastly, we present evidence that GFP-expressing U-87 cells migrating from a
660 tumorsphere can be challenged by cannflavin B in the low μM range as they infiltrate
661 human iPSC-derived cerebral organoids. Although we could not obtain precise quantitative
662 measures of GBM cell infiltration into the cerebral organoid structure using thin frozen
663 sections, we found that the tumorsphere size was significantly smaller after 10 days of
664 exposure to cannflavin B than after exposure to DMSO (vehicle control). This result calls
665 for a deeper investigation into the therapeutic value of cannflavin B against GBM or the
666 brain metastasis of other cancer types using live animal approaches, as mentioned above.
667 Corroborating the effectiveness of cannflavin B at limiting cancer progression with future
668 animal models would advance our research towards the design and proposal of a clinical
669 trial with human patients.

670 In conclusion, the distinctive ability of cannflavins, particularly cannflavin B, to
671 inhibit GBM cell migration and invasion, combined with their restrained cytotoxicity,
672 positions them as promising candidates for developing novel therapeutic strategies against

673 GBM. Future studies should focus on validating these effects in animal models to
674 understand the pharmacokinetics, bioavailability, and therapeutic index of cannflavins.
675 Furthermore, exploring the synergistic impact of cannflavins with existing
676 chemotherapeutic agents or targeted therapies could provide valuable insights into their
677 potential as adjuvant treatments, particularly in overcoming drug resistance—a significant
678 challenge in the management of GBM. Combining cannflavins with agents like TMZ
679 (Stupp et al., 2005; Stupp et al., 2009; Fisher et al., 2013) or the anti-angiogenic agent
680 bevacizumab (Fu et al., 2023) could enhance their therapeutic efficacy by simultaneously
681 targeting multiple aspects of tumor growth and invasion.

DATA AVAILABILITY

All data collected for the study are available upon inquiry to the corresponding author.

CONSENT FOR PUBLICATION

Consent to publish the article has been obtained from all authors.

FUNDING

This work was supported by Mitacs (Mitacs Elevate Program, IT29490) and the Canadian Foundation for Innovation (CFI, 037755). J.H. was also supported by a Queen Elizabeth II Graduate Scholarship in Science and Technology.

CREDIT AUTHORSHIP CONTRIBUTION STATEMENT

Jennifer Holborn: Conceptualization, Data curation, Formal analysis, Funding acquisition, Investigation, Writing – original draft, **Hannah Robeson:** Data curation, Methodology, Writing – review & editing. **Ellis Chartley:** Formal analysis, Methodology, Writing – review & editing. **Tiana Gluscevic**: Data curation, Methodology. **Adina Borenstein:** Methodology. **Colby Perrin:** Methodology. **Begüm Alural:** Methodology. **Himain Perera:** Visualization, Writing – review & editing. **Tariq A. Akhtar:** Resources. **Nina Jones:** Resources, Writing – review & editing. **Jasmin Lalonde:** Conceptualization, Data curation, Funding acquisition, Supervision, Writing – original draft.

DECLARATION OF COMPETING INTEREST

The other authors declare that they have no known competing financial interests or personal relationships that could have appeared to influence the work reported in this paper.

ACKNOWLEDGMENTS

We acknowledge the support of our lab colleagues in the development of this project.

SUPPLEMENTARY MATERIALS

Fig. S1 Cannflavin family members.

Fig. S2 LDH assay and TUNEL assay.

Fig. S3 Chrysoeriol and techtochrysin survival assay.

Supplementary Video. Scratch migration assay video.

714 **REFERENCES**

715 Balakrishnan, S., Bhat, F. A., Raja Singh, P., Mukherjee, S., Elumalai, P., Das, S., Patra,
716 C. R., Arunakaran, J., 2016. Gold nanoparticle–conjugated quercetin inhibits
717 epithelial–mesenchymal transition, angiogenesis and invasiveness via
718 EGFR/VEGFR-2-mediated pathway in breast cancer. Cell Prolif. 49, 678–697.
719 https://doi.org/10.1111/cpr.12296.

720 Barbaro, M., Blinderman, C.D., Iwamoto, F.M., Kreisl, T.N., Welch, M.R., Odia, Y.,
721 Donovan L.E., Joanta-Gomez, A.E., Evans, K.A., Lassman, A.B., 2022. Causes of
722 death and end-of-life care in patients with intracranial high-grade gliomas.
723 Neurology. 98, e260-e266. https://doi:10.1212/WNL.0000000000013057.

724 Barrett, M.L., Gordon, D., Evans, F.J., 1985. Isolation from Cannabis sativa L. of
725 cannflavin—a novel inhibitor of prostaglandin production. 34, 2019–2024.
726 http://doi:10.1016/0006-2952(85)90325-9.

727 Birzu C, French P, Caccese M, Cerretti G, Idbaih A, Zagonel V, Lombardi G., 2020.
728 Recurrent glioblastoma: From molecular landscape to new treatment perspectives.
729 Cancers (Basel). 13, 47. https://doi.org/10.3390/cancers13010047.

730 Cahill, K.E., Morshed, R.A., Yamini, B., 2016. Nuclear factor-κB in glioblastoma:
731 insights into regulators and targeted therapy. Neuro Oncol. 2016 18, 329–
732 339. https://doi.org/10.1093/neuonc/nov265.

733 Cazorla, M., Prémont, J., Mann, A., Girard, N., Kellendonk, C., Rognan, D., 2011.
734 Identification of a low-molecular weight TrkB antagonist with anxiolytic and
735 antidepressant activity in mice. J. Clin. Invest. 121, 1846–1857.
736 https://doi:10.1172/JCI43992.

737 Cheng, W.Y., Chiao, M.T., Liang, Y.J., Yang, Y.C., Shen, C.C., Yang, C.Y., 2013.
738 Luteolin inhibits migration of human glioblastoma U-87 MG and T98G cells through
739 downregulation of Cdc42 expression and PI3K/AKT activity. Mol. Biol. Rep. 40,
740 5315–5326. https://doi.org/10.1007/s11033-013-2632-1.
741 Choi, E.J., Bae, S.M., Ahn, W.S., 2008. Antiproliferative effects of quercetin through cell
742 cycle arrest and apoptosis in human breast cancer MDA-MB-453 cells. Arch. Pharm.
743 Res. 31, 1281–1285. https://doi.org/10.1007/s12272-001-2107-0.
744 Friedmann-Morvinski, D., Narasimamurthy, R., Xia, Y., Myskiw, C., Soda, Y., Verma,
745 I.M., 2016. Targeting NF-κB in glioblastoma: A therapeutic approach. Sci. Adv. 2,
746 e1501292. https://doi.org/10.1126/sciadv.1501292.
747 Eggers, C., Fujitani, M., Kato, R., Smid, S., 2019. Novel cannabis flavonoid, cannflavin
748 A displays both a hormetic and neuroprotective profile against amyloid β-mediated
749 neurotoxicity in PC12 cells: Comparison with geranylated flavonoids, mimulone and
750 diplacone. Biochem. Pharmacol., 169. https://doi.org/10.1016/j.bcp.2019.08.011.
751 Erdogan, S., Doganlar, O., Doganlar, Z.B., Serttas, R., Turkekul, K., Dibirdik, I., Bilir,
752 A., 2016. The flavonoid apigenin reduces prostate cancer CD44+ stem cell survival
753 and migration through PI3K/Akt/NF-κB signaling. Life Sci. 162, 77–86.
754 https://doi.org/10.1016/j.lfs.2016.08.019.
755 Fisher J.P., Adamson D.C., 2021. Current FDA-approved therapies for high-grade
756 malignant gliomas. Biomedicines. 9, 324.
757 https://doi.org/10.3390/biomedicines9030324.

758 Fu., M., Zhou, Z., Huang, X., Chen, Z., Zhang, L., Zhang, J., Hua. W., Mao, Y., 2023.
759 Use of Bevacizumab in recurrent glioblastoma: a scoping review and evidence map.
760 BMC Cancer. 23, 544. https://doi.org/10.1186/s12885-023-11043-6.
761 Gaetani, M., Sabatier, P., Saei, A.A., Beusch, C.M., Yang, Z., Lundström, S.L., Zubarev,
762 R.A., 2019. Proteome integral solubility alteration: A high-throughput proteomics
763 assay for target deconvolution. J. Proteome Res. 18, 4027–4037.
764 https://doi.org/10.1021/acs.jproteome.9b00500.
765 Gaetani, M., Zubarev, R.A., 2023. Proteome Integral Solubility Alteration (PISA) for
766 high-throughput ligand target deconvolution with increased statistical significance
767 and reduced sample amount. Methods Mol. Biol. 2554, 91–106.
768 https://doi.org/10.1007/978-1-0716-2624-5_7.
769 Gao, X., Wang, B., Wei, X., Men, K., Zheng, F., Zhou, Y., Zheng, Y., Gou, M., Huang,
770 M., Guo, G., Huang, N., Qian, Z., Wei, Y., 2012. Anticancer effect and mechanism
771 of polymer micelle-encapsulated quercetin on ovarian cancer. Nanoscale, 4, 7021–
772 7030. https://doi.org/10.1039/c2nr32181e.
773 Gao, Y., Yin, J., Rankin, G.O., Chen, Y.C., 2018. Kaempferol induces G2/M cell cycle
774 arrest via checkpoint kinase 2 and promotes apoptosis via death receptors in human
775 ovarian carcinoma A2780/CP70 cells. Molecules, 23, 1095.
776 https://doi.org/10.3390/molecules23051095.
777 Gómez-Oliva, R., Domínguez-García, S., Carrascal, L., Abalos-Martínez, J., Pardillo-
778 Díaz, R., Verástegui, C., Castro, C., Nunez-Abades, P., Geribaldi-Dolbán, N., 2021.
779 Evolution of experimental models in the study of glioblastoma: Toward finding

780 efficient treatments. Front. Oncol., 10, 614295.
781 https://doi:10.3389/fonc.2020.614295.
782 Haddad, A.F., Young, J.S., Amara, D., Berger, M.S., Raleigh, D.R., Aghi, M., Butowski,
783 N.A., 2021. Mouse models of glioblastoma for the evaluation of novel therapeutic
784 strategies. Neurooncol. Adv., **b**, vdab100. https://doi:10.1093/noajnl/vdab100.
785 Holborn J, Walczyk-Mooradally A, Perrin C, Alural B, Aitchison C, Borenstein A, Jones
786 N, Khokhar J.Y., Akhtar T.A., Lalonde J., 2023. Interference of neuronal TrkB
787 signaling by the cannabis-derived flavonoids cannflavins A and B. Phytomed. Plus.
788 3, 100410. https://doi.org/10.1016/j.phyplu.2023.100410.
789 Huang, L., Jin, K., Lan, H., 2019. Luteolin inhibits cell cycle progression and induces
790 apoptosis of breast cancer cells through downregulation of human telomerase reverse
791 transcriptase. Oncol. Lett. 17, 3842–3850. https://doi.org/10.3892/ol.2019.10052.
792 Jo, E., Park, S.J., Choi, Y.S., Jeon, W.K., Kim, B.C., 2015. Kaempferol suppresses
793 transforming growth factor-β1-induced epithelial-to-mesenchymal transition and
794 migration of A549 lung cancer cells by inhibiting Akt1-mediated phosphorylation of
795 Smad3 at threonine-179. Neoplasia. 17, 525–537.
796 https://doi.org/10.1016/j.neo.2015.06.004.
797 Johnson, D.R., O'Neill, B.P., 2012. Glioblastoma survival in the United States before and
798 during the temozolomide era. J. Neuro-Oncol. 107, 359–364.
799 https://doi.org/10.1007/s11060-011-0749-4.
800 Khan, A., Zhang, Y., Ma, N., Shi, J., Hou, Y., 2024 NF-κB role on tumor proliferation,
801 migration, invasion and immune escape. Cancer Gene Ther. 31, 1599–1610.
802 https://doi.org/10.1038/s41417-024-00811-6.

803 Kim, S. H., Yoo, E.S., Woo, J.S., Han, S.H., Lee, J.H., Jung, S.H., Kim, H.J., Jung, J.Y.,
804 2019. Antitumor and apoptotic effects of quercetin on human melanoma cells
805 involving JNK/P38 MAPK signaling activation. Eur. J. Pharmacol. 860:172568.
806 https://doi.org/10.1016/j.ejphar.2019.172568.
807 Lalonde, J., Reis, S.A., Sivakumaran, S., Holland, C.S., Wesseling, H., Sauld, J., Alural,
808 B., Zhao, W.N., Steen, J., Haggarty, S.J., 2017. Chemogenomic analysis reveals key
809 role for lysine acetylation in regulating Arc protein stability. Nat. Commun. 8:1659.
810 https://doi.org/10.1038/s41467-017-01750-7.
811 Lau, H.R., Alural, B., Martin, C.E., New, L.A., Smith, H.S., Tilak, M., Banerjee, S.L.,
812 Robeson, H.N., Bisson, N., Gingras, A.C., Lalonde J, Jones, N., 2025. ShcD adaptor
813 protein drives invasion of triple-negative breast cancer cells by aberrant activation of
814 EGFR signaling. Mol. Oncol. Mar. 28, https://doi.org/10.1002/1878-0261.70022.
815 Lee, W.J., Hsiao, M., Chang, J.L., Yang, S.F., Tseng, T.H., Cheng, C.W., Chow, J.M.,
816 Lin, K.H., Lin, Y.W., Liu, C.C., Lee, L.M., Chien, M.H., 2015. Quercetin induces
817 mitochondrial-derived apoptosis via reactive oxygen species-mediated ERK
818 activation in HL-60 leukemia cells and xenograft. Arch. Toxicol. 89, 1103–1117.
819 https://doi.org/10.1007/s00204-014-1300-0.
820 Li, Y., Liu, F., Cai, Q., Deng, L., Ouyang, Q., Zhang, X.H.F., Zheng, J., 2025. Invasion
821 and metastasis in cancer: molecular insights and therapeutic targets. Signal
822 Transduct. Target. Ther. 10, 57. https://doi.org/10.1038/s41392-025-02148-4.
823 Li, S., Yan, T., Deng, R., Jiang, X., Xiong, H., Wang, Y., Yu, Q., Wang, X., Chen, C.,
824 Zhu, Y., 2017. Low dose of kaempferol suppresses the migration and invasion of

825 triple-negative breast cancer cells by downregulating the activities of RhoA and
826 Rac1. Onco Targets Ther. 10, 4809–4819. https://doi.org/10.2147/OTT.S140886.
827 Lin, C.H., Chang, C.Y., Lee, K.R., Lin, H.J., Chen, T.H., Wan, L., 2015. Flavones inhibit
828 breast cancer proliferation through the Akt/FOXO3a signaling pathway. BMC
829 Cancer. 15, 958. https://doi.org/10.1186/s12885-015-1965-7.
830 Linkous, A., Balamatsias, D., Snuderl, M., Edwards, L., Miyaguchi, K., Milner, T.,
831 Reich, B., Cohen-Gould, L., Storaska, A., Nakayama, Y., Schenkein, E., Singhania,
832 R., Cirigliano, S., Magdeldin, T., Lin, Y., Nanjangud, G., Chadalavada, K., Pisapia,
833 D., Liston, C., Fine, H.A., 2019. Modeling Patient-Derived Glioblastoma with
834 Cerebral Organoids. Cell Rep., 26, 3203–3211.
835 Moreau, M., Ibeh, U., Decosmo, K., Bih, N., Yasmin-Karim, S., Toyang, N., Lowe, H.,
836 Ngwa, W., 2019. Flavonoid derivative of cannabis demonstrates therapeutic potential
837 in preclinical models of metastatic pancreatic cancer. Front. Oncol. 9, 660.
838 https://doi.org/10.3389/fonc.2019.00660.
839 Nagai, S., Washiyama, K., Kurimoto, M., Takaku, A., Endo, S., Kumanishi, T., 2002.
840 Aberrant nuclear factor-kB activity and its participation in the growth of human
841 malignant astrocytoma. J. Neurosurg. 96, 909–917.
842 https://doi.org/10.3171/jns.2002.96.5.0909.
843 Ostrom, Q.T., Patil, N., Cioffi, G., Waite, K., Kruchko, C., Barnholtz-Sloan J.S., 2020.
844 CBTRUS Statistical Report: Primary brain and other central nervous System tumors
845 diagnosed in the United States in 2013–2017. Neuro-Oncol., 22, iv1–iv96.
846 https://doi.org/10.1093/neuonc/noaa200.

847 Panche, A.N., Diwan, A.D., Chandra, S.R., 2016. Flavonoids: An overview. J. Nutr.
848 Sci. 5, e47. https://doi:10.1017/jns.2016.41.
849 Park, M.H., Hong, J.E., Park, E.S., Yoon, H.S., Seo, D.W., Hyun, B.K., 2015. Anticancer
850 effect of tectochrysin in colon cancer cell via suppression of NF-kappaB activity and
851 enhancement of death receptor expression. Mol. Cancer. 14:124
852 https://doi:10.1186/s12943-015-0377-2.
853 Pinheiro, K. V., Alves, C., Buendia, M., Gil, M. S., Thomaz, A., Schwartsmann, G., De
854 Farias, C. B., & Roesler, R., 2017. Targeting tyrosine receptor kinase B in gliomas.
855 Neuro. Oncol. 19, 138–139. https://doi.org/10.1093/neuonc/now199.
856 Pratheeshkumar, P., Budhraja, A., Son, Y.O., Wang, X., Zhang, Z., Ding, S., Wang, L.,
857 Hitron, A., Lee, J.C., Xu, M., Chen, G., Luo, J., Shi, X., 2012. Quercetin inhibits
858 angiogenesis mediated human prostate tumor growth by targeting VEGFR-2
859 regulated AKT/mTOR/P70S6K signaling pathways. PLoS ONE, 7, e47516.
860 https://doi.org/10.1371/journal.pone.0047516.
861 Raychaudhuri, B., Han, Y., Lu, T., Vogelbaum, M.A., 2007. Aberrant constitutive
862 activation of nuclear factor kappaB in glioblastoma multiforme drives invasive
863 phenotype. J. Neurooncol. 85, 39–47. https://doi.org/10.1007/s11060-007-9390-7.
864 Rea, K.A., Casaretto, J.A., Al-Abdul-Wahid, M.S., Sukumaran, A., Geddes-McAlister, J.,
865 Rothstein, S.J., & Akhtar, T.A., 2019. Biosynthesis of cannflavins A and B from
866 Cannabis sativa L. *Phytochemistry*, *164*, 162–171.
867 https://doi.org/10.1016/j.phytochem.2019.05.009.
868 Srivastava, S., Somasagara, R.R., Hegde, M., Nishana, M., Tadi, S.K., Srivastava, M.,
869 Choudhary, B., Raghavan, S.C., 2016. Quercetin, a natural flavonoid interacts with

870 DNA, arrests cell cycle and causes tumor regression by activating mitochondrial
871 pathway of apoptosis. Sci. Rep. 6, 24049. https://doi.org/10.1038/srep24049.
872 Stupp, R., Mason, W.P., Bent, M.J. van den, Weller M., Fisher, B., Taphoorn, M.J.B.,
873 Belanger, K., Brandes, A.A., Marosi, C., Bogdahn, U., Curschmann, J., Janzer, R.C.,
874 Ludwin, S.K., Gorlia, T., Allgeier, A., Lacombe, D., Cairncross, J.G., Eisenhauer, E.,
875 Mirimanoff, R.O., European Organisation for Research and Treatment of Cancer
876 Brain Tumor and Radiotherapy Groups; National Cancer Institute of Canada Clinical
877 Trials Group., 2005. Radiotherapy plus concomitant and adjuvant temozolomide for
878 glioblastoma. N. Engl. J. Med. 2352, 987–996.
879 https://doi.org/10.1056/nejmoa043330.
880 Stupp, R., Hegi, M.E., Mason, W.P., Bent, M.J. van den, Taphoorn, M.J., Janzer, R.C.,
881 Ludwin, S.K., Allgeier, A, Fisher, B., Belanger, K., Hau, P., Brandes, A.A.,
882 Gijtenbeek, J., Marosi, C., Vecht, C.J., Mokhtari, K., Wesseling, P., Villa, S.,
883 Eisenhauer, E., Gorlia, T., Weller, M., Lacombe, D., Cairncross, J.G., Mirimanoff,
884 R.O; European Organisation for Research and Treatment of Cancer Brain Tumour
885 and Radiation Oncology Groups; National Cancer Institute of Canada Clinical Trials
886 Group, 2009. Effects of radiotherapy with concomitant and adjuvant temozolomide
887 versus radiotherapy alone on survival in glioblastoma in a randomised phase III
888 study: 5-year analysis of the EORTC-NCIC trial. Lancet Oncol. 10, 459–466.
889 https://doi.org/10.1016/s1470-2045(09)70025-7.
890 Taniguchi, K., Karin, M., 2018. NF-κB, inflammation, immunity and cancer: coming of
891 age. Nat. Rev. Immunol. 18, 309–324. https://doi.org/10.1038/nri.2017.142.

892 Tilak, M., Alural, B., Holborn, J., Lalonde, J., Jones, N., 2021a. Receptor tyrosine kinase
893 signaling and targeting in glioblastoma. Int. J. Mol. Sci. 22, 1831.
894 https://doi:10.3390/ijms22041831.
895 Tilak, M., Alural, B., Wismer, S.E., Brasher, M.I., New, L.A., Sheridan, S.D., Perlis,
896 R.H., Coppolino, M.G., Lalonde, J., Jones, N., 2021b. Adaptor protein ShcD/SHC4
897 interacts with tie2 receptor to synergistically promote glioma cell invasion. Mol.
898 Cancer Res. 19, 757–770. https://doi.org/10.1158/1541-7786.MCR-20-0188.
899 Tomko, A.M., Whynot, E.G., Dupré, D.J., 2022. Anti-cancer properties of cannflavin A
900 and potential synergistic effects with gemcitabine, cisplatin, and cannabinoids in
901 bladder cancer. J. Cannabis Res. 4, 41. https://doi.org/10.1186/s42238-022-00151-y.
902 Tseng, T.H., Chien, M.H., Lin, W.L., Wen, Y.C., Chow, J.M., Chen, C.K., Kuo, T.C.,
903 Lee, W.J., 2017. Inhibition of MDA-MB-231 breast cancer cell proliferation and
904 tumor growth by apigenin through induction of G2/M arrest and histone H3
905 acetylation-mediated p21WAF1/CIP1 expression. Environ. Toxicol. 32, 434–444.
906 https://doi.org/10.1002/tox.22247.
907 Vinci, M., Box, C., Eccles, S.A., 2015. Three-dimensional (3D) tumor spheroid invasion
908 assay. J. Vis. Exp. 99, e52686. https://doi.org/10.3791/52686.
909 Wang, X., Sun, Y., Zhang, D.Y., Ming, G., Song, H., 2023. Glioblastoma modeling with
910 3D organoids: progress and challenges. Oxf. Open Neurosci. 2, kvad008.
911 https://doi:10.1093/oons/kvad008.
912 Wang, H., Wang, H., Zhang, W., Huang, H.J., Liao, W.S., Fuller, G.N. 2004. Analysis of
913 the activation status of Akt, NFkappaB, and Stat3 in human diffuse gliomas. Lab
914 Invest. 84, 941–951. https://doi.org/10.1038/labinvest.3700123.

915 Weller M, Cloughesy T, Perry J.R., Wick W., 2013. Standards of care for treatment of
916 recurrent glioblastoma—are we there yet? Neuro Oncol. 15, 4–27.
917 https://doi.org/10.1093/neuonc/nos273.
918 Werz, O., Seegers, J., Schaible, A.M., Weinigel, C., Barz, D., Koeberle, A., Allegrone,
919 G., Pollastro, F., Zampieri, L., Grassi, G., Appendino, G., 2014. Cannflavins from
920 hemp sprouts, a novel cannabinoid-free hemp food product, target microsomal
921 prostaglandin E_2 synthase-1 and 5-lipoxygenase. PharmaNutrition. 2, 53–60.
922 https://doi.org/10.1016/j.phanu.2014.05.001.
923 Zhang, Q., Cheng, G., Qiu, H., Wang, Y., Wang, J., Xu, H., Zhang, T., Liu, L., Tao, Y.,
924 Ren, Z., 2017. Expression of prostate stem cell antigen is downregulated during
925 flavonoid-induced cytotoxicity in prostate cancer cells. Exp. Ther. Med. 14, 1795–
926 1801. https://doi.org/10.3892/etm.2017.4638.
927 Zhang, T., Ma, C., Zhang, Z., Zhang, H., Hu, H., 2021 NF-κB signaling in inflammation
928 and cancer. MedComm. 2, 618–653. https://doi.org/10.1002/mco2.104.
929 Zhu, L., Xue, L., 2019. Kaempferol suppresses proliferation and induces cell cycle arrest,
930 apoptosis, and DNA damage in breast cancer cells. Oncol. Res. 27, 629–634.
931 https://doi.org/10.3727/096504018X15228018559434.

932 **FIGURE 1**

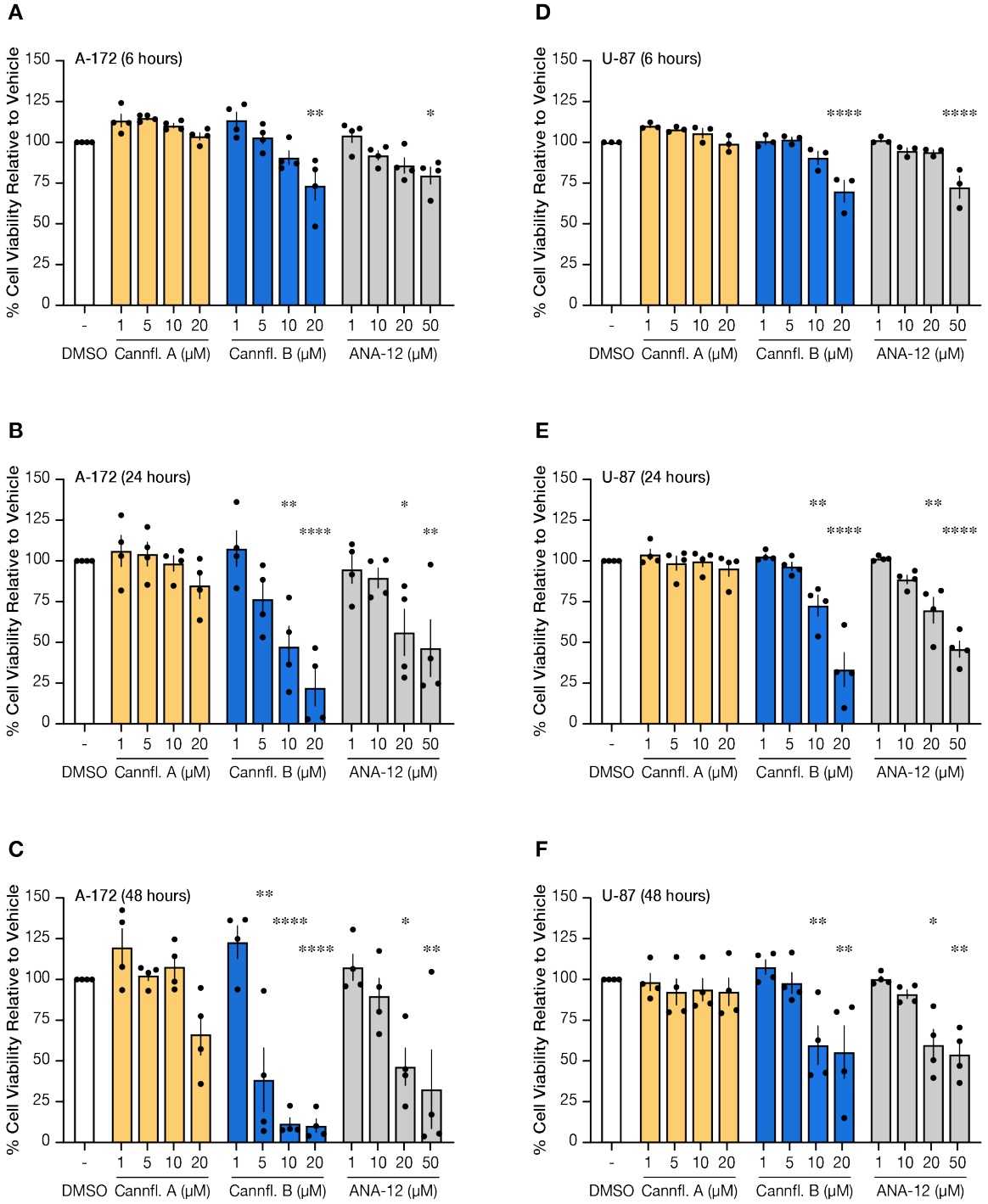

933

934 **Figure 1.** Cannflavin B reduces GBM cell viability. A172 **(A-C)** and U-87 **(D-F)** cells

935 were treated with increased concentrations of cannflavin A (1-20 μM), cannflavin B (1-20

936 μM), or ANA-12 (1-50 μM) and cell viability was measured at 24-, 48-, and 72-hour time-

937 points using the resazurin reduction assay. DMSO was used as a vehicle control.
938 Application of cannflavin B and ANA-12, but not cannflavin A, reduced the viability of
939 both A-172 and U-87 GBM cells in a dose- and time-dependent manner. A one-way
940 ANOVA was used to analyze the data from each cell line, treatment, and time point
941 independently with DMSO as the reference control. Tukey's honestly significant
942 difference (HSD) post hoc test: * $p < 0.05$, ** $p < 0.01$, *** $p < 0.001$, **** $p < 0.0001$.
943 Graphs represent mean ± SEM (n = 3-4).

944 **FIGURE 2**

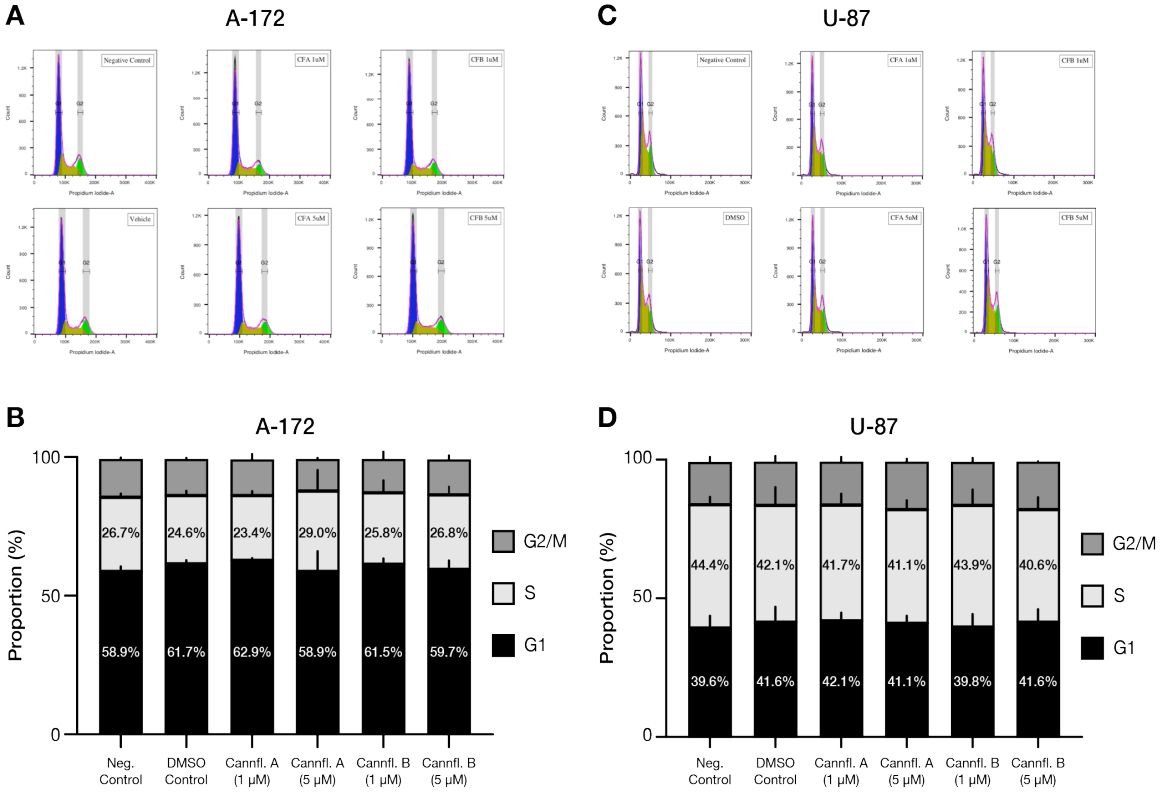

945

946 **Figure 2. Cannflavins A and B did not affect cell cycle distribution in GBM cell lines.**

947 A-172 **(A-B)** and U-87 **(C-D)** DNA content was determined by gating on the G1, S, and

948 G2/M phases using flow cytometry and analyzed using the Watson Pragmatic algorithm to

949 distribute cell cycle phases. A172 **(B)** and U-87 **(D)** cell cycle data are expressed as mean

950 ± SEM (n = 3).

951 **FIGURE 3**

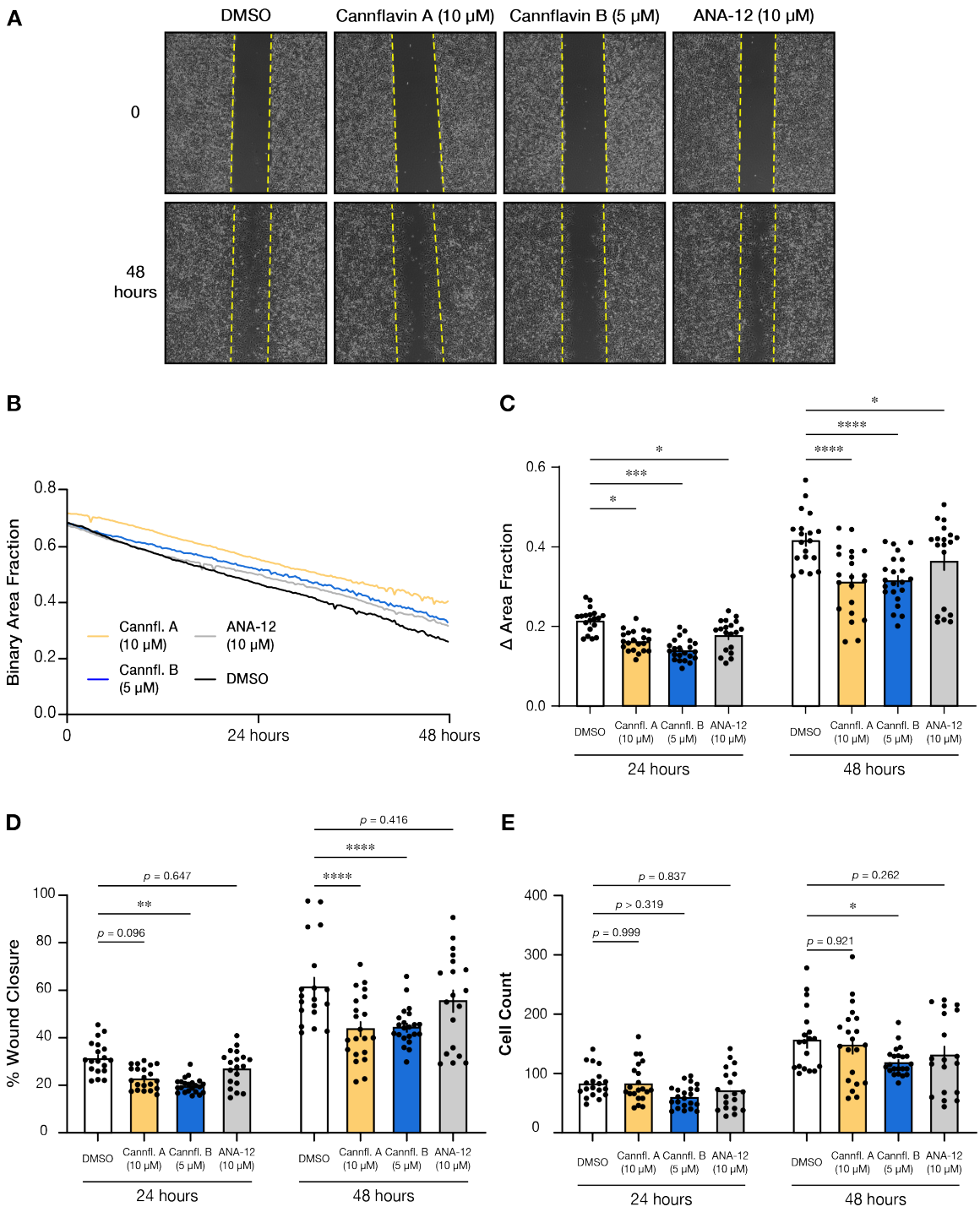

952

953 **Figure 3.** Cannflavins A and B suppress A-172 cell migration. **(A)** Representative phase-

954 contrast images of scratch assay showing A-172 GBM cancer cells within a gap created

955 with a pipette tip at 0 hour and 48 hours. Dashed yellow lines indicate the initial wound

edges. **(B)** Quantification of the binary wound area fraction over time, showing delayed wound closure in inhibitor-treated conditions. **(C)** Normalized wound area fraction at 24 hours and 48 hours. A two-way ANOVA reveals a significant effect of time ($F_{1,218} = 133.3$, $p < 0.0001$) as well as treatment ($F_{3,218} = 18.37$, $p < 0.0001$). There is no significant interaction between time and treatment ($F_{3,218} = 2.094$, $p = 0.1019$). Post hoc comparisons between DMSO control and each treatment means were conducted using Dunnett's multiple comparisons. All treatments at all time points produced a significant reduction in cell migration. **(D)** Percentage of wound closure at 24 hours and 48 hours. A two-way ANOVA reveals a significant effect of time ($F_{1,218} = 104.2$, $p < 0.0001$) as well as treatment ($F_{3,218} = 16.45$, $p < 0.0001$). There is no significant interaction between time and treatment ($F_{3,218} = 1.885$, $p = 0.133$). Post hoc comparisons between DMSO control and each treatment means were conducted using Dunnett's multiple comparisons. Cannflavin B significantly limited closure at both time points, while cannflavin A was significant only at 48 hours. ANA-12 did not cause a significant effect. **(E)** Total cell counts within the imaging field at 24 hours and 48 hours. A two-way ANOVA reveals a significant effect of time ($F_{1,154} = 92.25$, $p < 0.0001$) as well as treatment ($F_{3,154} = 4.46$, $p = 0.0049$). There is no significant interaction between time and treatment ($F_{3,154} = 0.2556$, $p = 0.8573$). Post hoc comparisons between DMSO control and each treatment means were conducted using Dunnett's multiple comparisons. Significantly less cells were found in the wound area with cannflavin B at 48 hours. No other comparisons were significantly different. All data represented as mean ± SEM (3 biological replicates with 6-8 images per well; * $p < 0.05$, ** $p < 0.01$, *** $p < 0.001$, **** $p < 0.0001$).

978 **FIGURE 4**

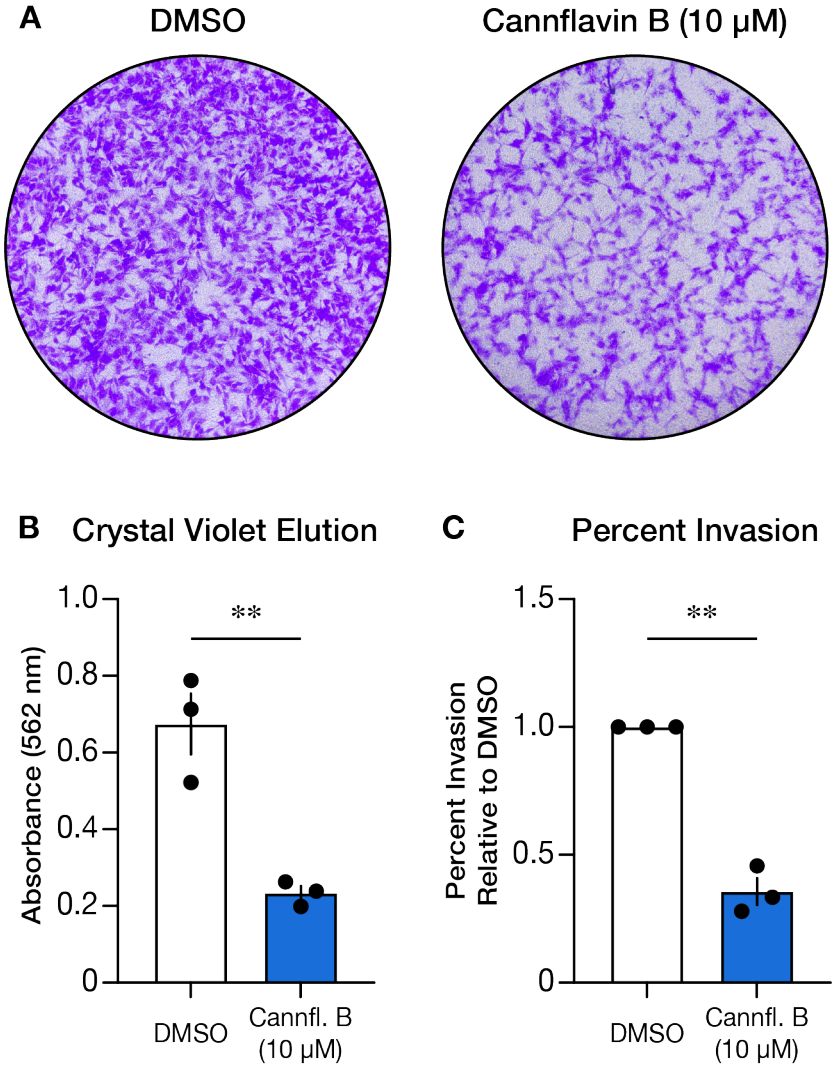

979

980 **Figure 4. Cannflavin B inhibits A-172 glioblastoma cell invasion in a transwell assay.**
981 **(A)** Representative images of stained migrated A-172 cells following treatment with
982 DMSO or cannflavin B (10 μM). **(B)** Quantification of migration using crystal violet
983 elution measured by absorbance at 562 nm. **(C)** Percent invasion between DMSO control
984 and cannflavin B, showing a significant reduction in cannflavin B-treated cells. Data
985 represent mean ± SEM, with statistical significance determined by an unpaired two-tailed
986 *t*-test (** $p < 0.01$).

987 **FIGURE 5**

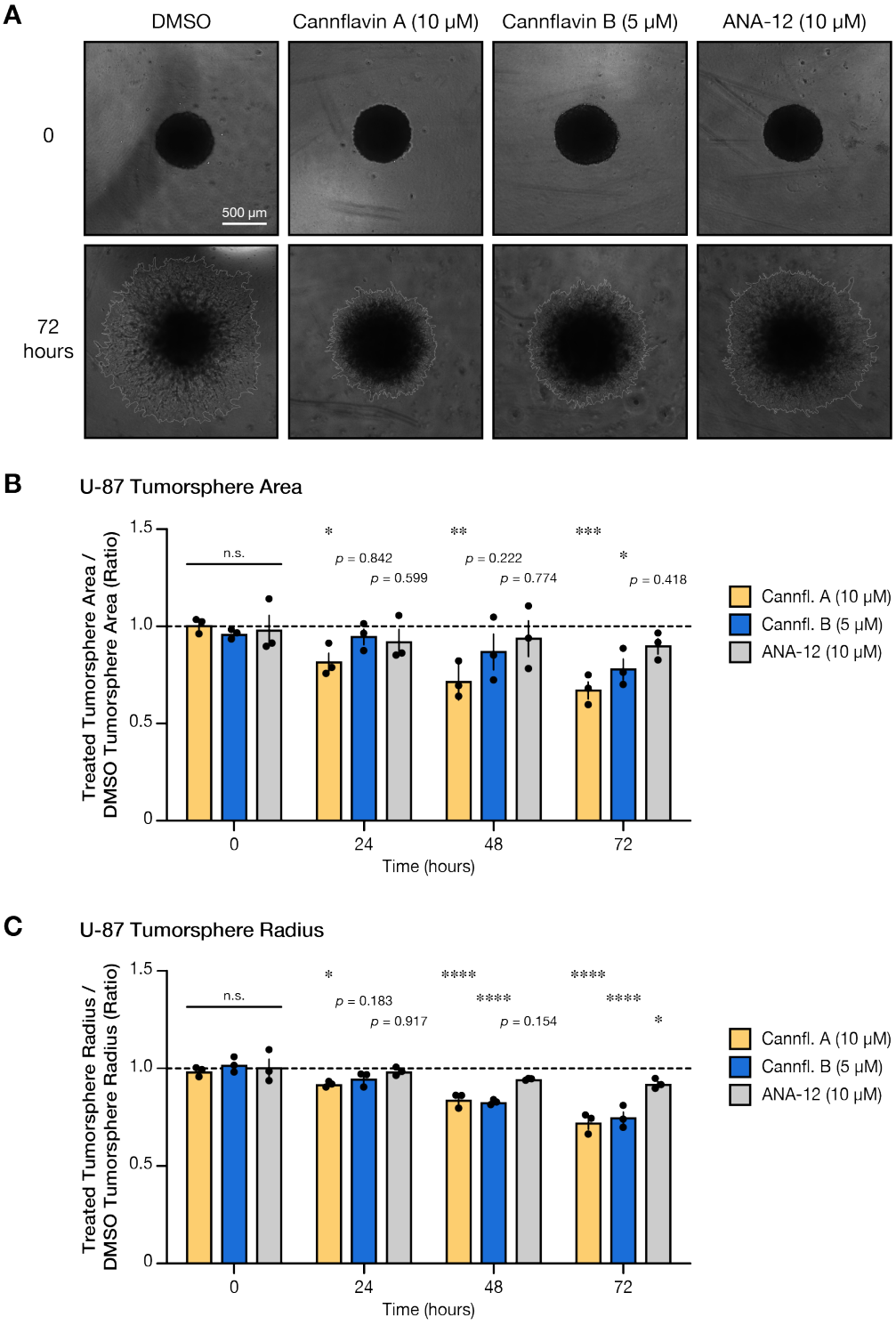

988

989 **Figure 5.** Cannflavins A and B inhibit the outgrowth of U-87 tumorspheres. **(A)**

990 Representative phase-contrast images of U-87 tumorspheres at 0 hour and 72 hours post-

991 treatment with DMSO (vehicle), ANA-12 (10 μM), cannflavin A (10 μM), or cannflavin
992 B (5 μM) in a tumorsphere invasion assay. Scale bar: 500 μm. The white outline indicates
993 the borders of tumorsphere outgrowth. **(B)** Quantification of relative tumorsphere area
994 expansion over time, normalized to the vehicle control. A two-way ANOVA reveals a
995 significant effect of time ($F_{3,32} = 5.949$, $p < 0.0024$) as well as treatment ($F_{3,32} = 10.13$, p
996 < 0.0001). There is no significant interaction between time and treatment ($F_{9,32} = 1.765$, p
997 $= 0.1145$). Post hoc comparisons between DMSO control and each treatment means were
998 conducted using Dunnett's multiple comparisons. Ratio was significantly lower at all three
999 time points for cannflavin A, while cannflavin B was significant only at 72 hours. ANA-
1000 12 did not cause a significant effect. **(C)** Relative tumorsphere radius expansion over time,
1001 showing significant inhibition of invasion upon cannflavin treatment. A two-way ANOVA
1002 reveals a significant effect of time ($F_{3,32} = 46.18$, $p < 0.0001$) as well as treatment ($F_{3,32} =$
1003 40.07, $p < 0.0001$). Notably, there is a significant interaction between time and treatment
1004 ($F_{9,32} = 8.749$, $p < 0.0001$), reflecting an earlier effect with cannflavin A, followed by
1005 cannflavin B, and finally ANA-12. Post hoc comparisons between DMSO control and each
1006 treatment means were conducted using Dunnett's multiple comparisons. Data represent
1007 mean ± SEM ($n = 3$; * $p < 0.05$; ** $p < 0.01$; *** $p < 0.001$; **** $p < 0.0001$; n.s., not
1008 significant).

1009 **FIGURE 6**

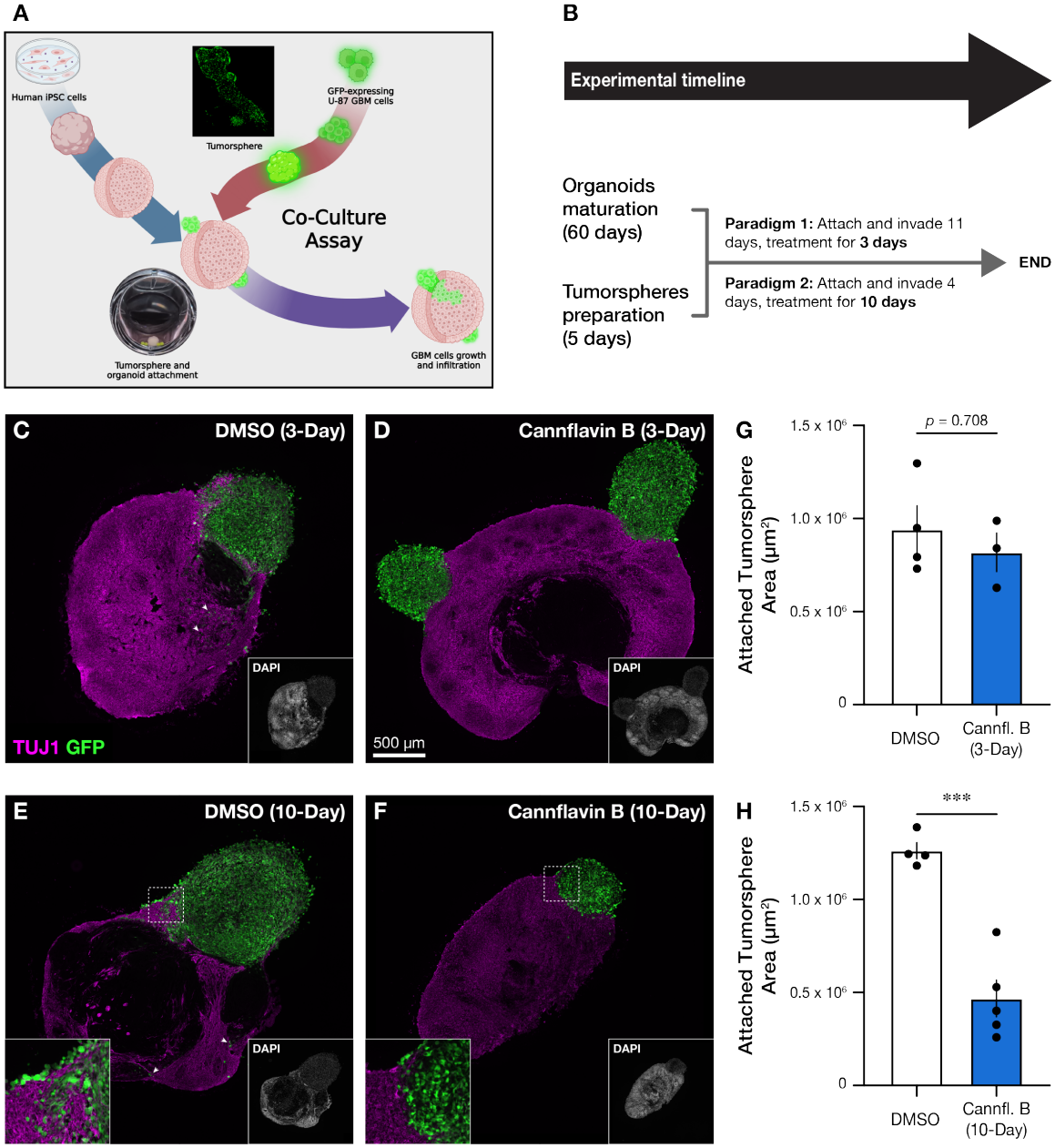

1010

1011 **Figure 6.** Cannflavin B reduces the size of attached tumorspheres to a cerebral organoid.
1012 **(A)** Schematic representation of cerebral organoid and U-87 tumorspheres co-culture
1013 model. Cerebral organoids matured for 60 days before introducing tumorspheres prepared
1014 with U-87 cells expressing GFP. **(B)** Two experimental timelines were tested: 11 days of
1015 co-culture followed by 3 days of applying cannflavin B to the culture media (final

1016 concentration of 5 μM), and 4 days of co-culture followed by 10 days of applying
1017 cannflavin B (final concentration of 5 μM). **(C-F)** Representative capture of organoid with
1018 attached tumorsphere(s) for all conditions. **(G-H)** Estimation of tumorsphere size in the 3-
1019 day **(G)** and 10-day **(H)** conditions. The average area of the tumorsphere (GFP-positive
1020 cells, green) was significantly smaller after 10 days of cannflavin B application compared
1021 to the corresponding DMSO control. Data represent mean ± SEM, with statistical
1022 significance determined by an unpaired two-tailed *t*-test (*** $p < 0.001$).

1023 **FIGURE 7**

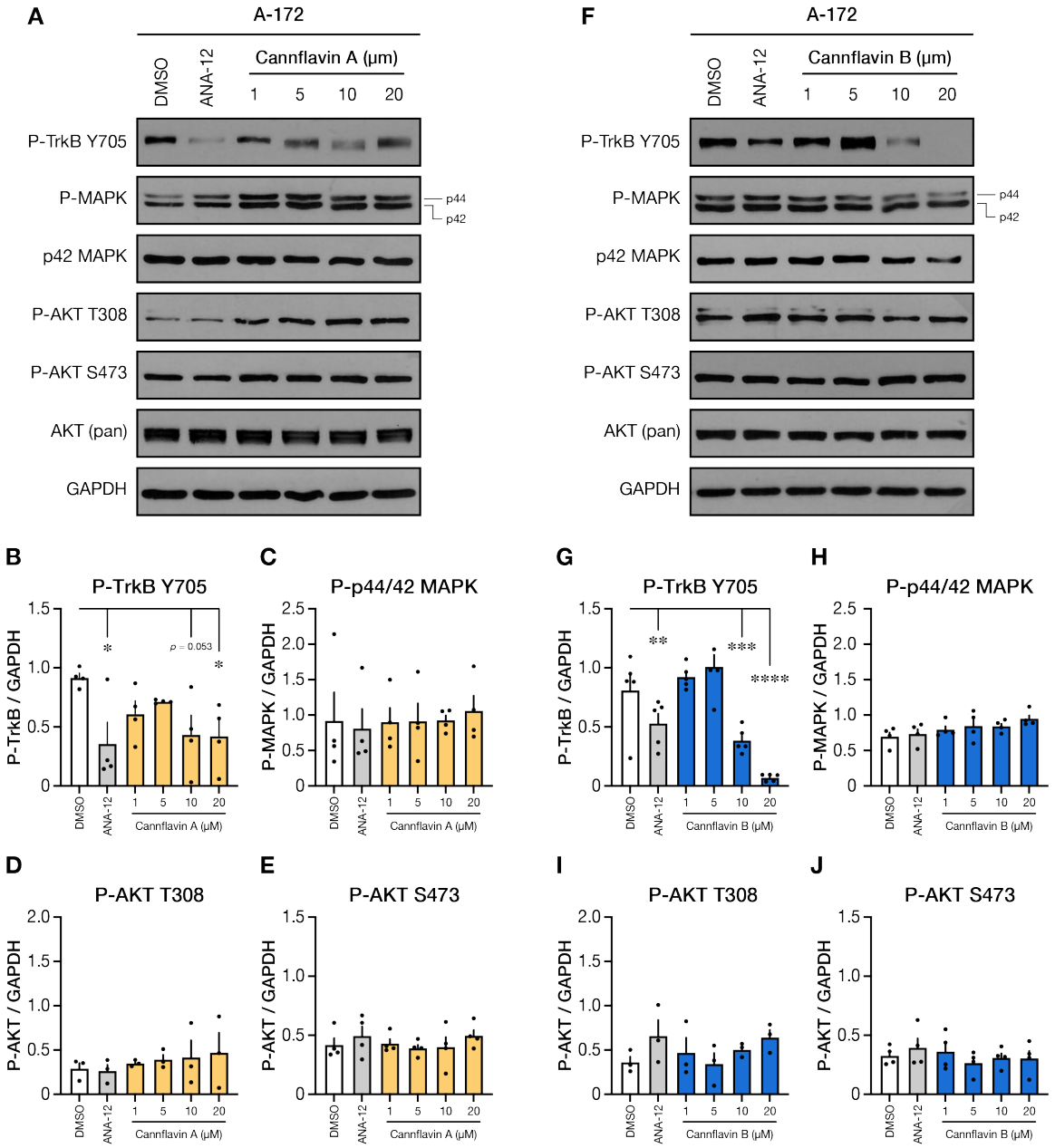

1024

1025 **Figure 7.** Cannflavin A and cannflavin B affect TrkB Y705 activation site but not
1026 downstream signaling in A-172 cells. Western blot analysis from A-172 cells treated for 6
1027 hours with cannflavin A **(A-E)** and cannflavin B **(F-J)** at various concentrations.
1028 Corresponding densitometry quantifications reveal a significant reduction in P-TrkB Y705
1029 signal, but not in P-MAPK and P-AKT. GAPDH (glyceraldehyde-3-phosphate

1030 dehydrogenase) was used as a loading control. Graphs show the mean ± SEM (n = 4) of
1031 the target/GAPDH ratio for cells treated as in **(A)** and **(F)**. Post hoc comparisons between
1032 DMSO control and each treatment means were conducted using Dunnett's multiple
1033 comparisons (* $p < 0.05$; ** $p < 0.01$; *** $p < 0.001$; **** $p < 0.0001$).

1034 **FIGURE 8**

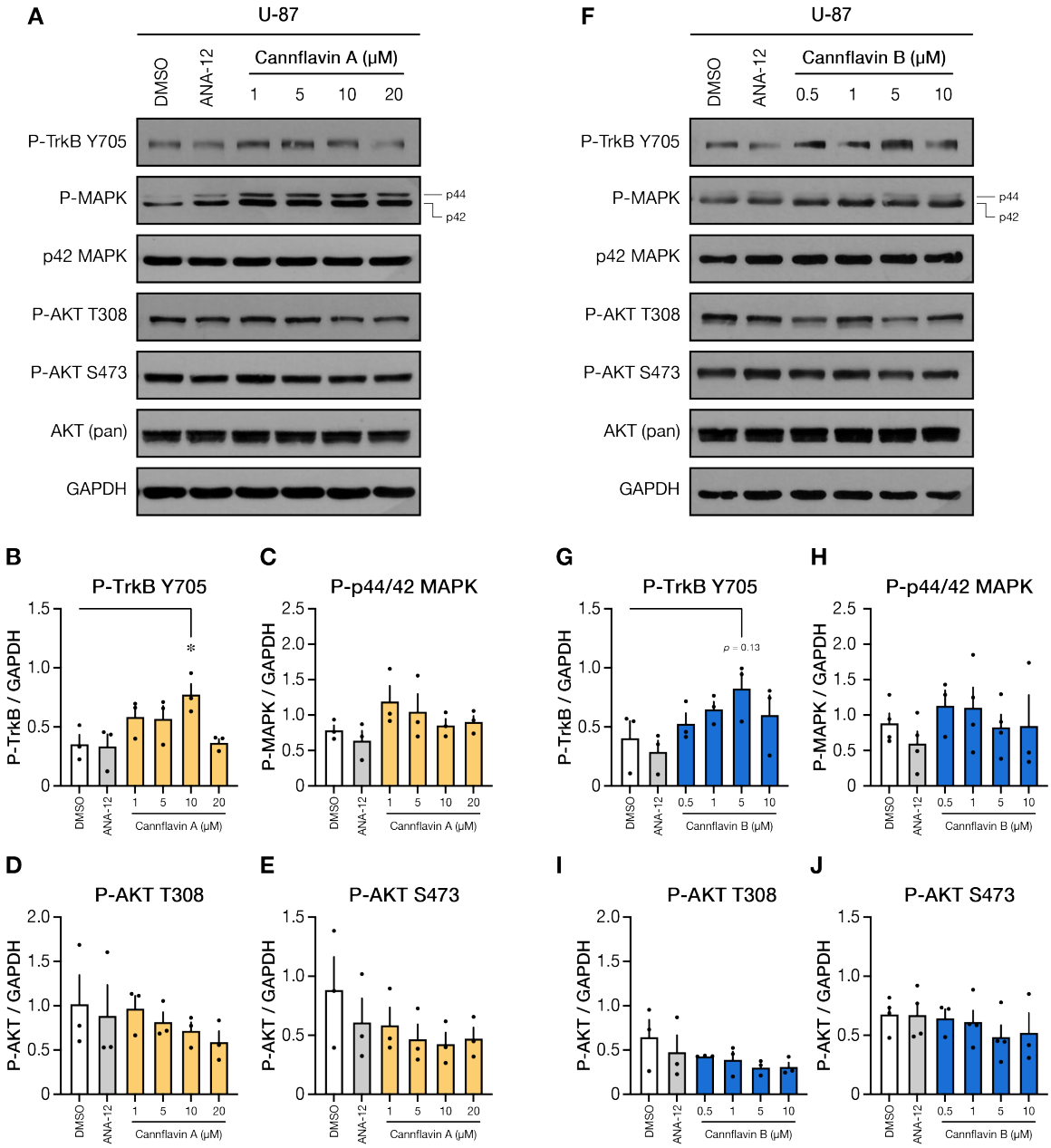

1035

1036 **Figure 8.** Cannflavin A and cannflavin B slightly increase TrkB Y705 activation site but
1037 not change downstream signaling in U-87 cells. Western blot analysis from U-87 cells
1038 treated for 6 hours with cannflavin A **(A-E)** and cannflavin B **(F-J)** at various
1039 concentrations. Corresponding densitometry quantifications reveal a significant reduction
1040 in P-TrkB Y705 signal, but not in P-MAPK and P-AKT. GAPDH (glyceraldehyde-3-

1041 phosphate dehydrogenase) was used as a loading control. Graphs show the mean ± SEM
1042 (n = 3) of the target/GAPDH ratio for cells treated as in **(A)** and **(F)**. Post hoc comparisons
1043 between DMSO control and each treatment means were conducted using Dunnett's
1044 multiple comparisons (* $p < 0.05$).

Supplementary Information for

Preclinical Study of Cannflavins A and B Action Against Glioblastoma Cells

Jennifer Holborn [a], Hannah Robeson [a,1], Ellis Chartley [a,1], Tiana Gluscevic [a,b,1], Adina Borenstein [a], Colby Perrin [a], Begüm Alural [a], Himain Perera [a], Tariq A. Akhtar [a], Nina Jones [a], Jasmin Lalonde [a,*]

* Correspondence to: jlalon07@uoguelph.ca

This PDF file includes:

Fig. S1 Cannflavin family members.

Fig. S2 LDH assay and TUNEL assay.

Fig. S3 Chrysoeriol and techtochrysin survival assay.

Supplementary Video. Scratch migration assay video.

SUPPLEMENTARY FIGURE 1

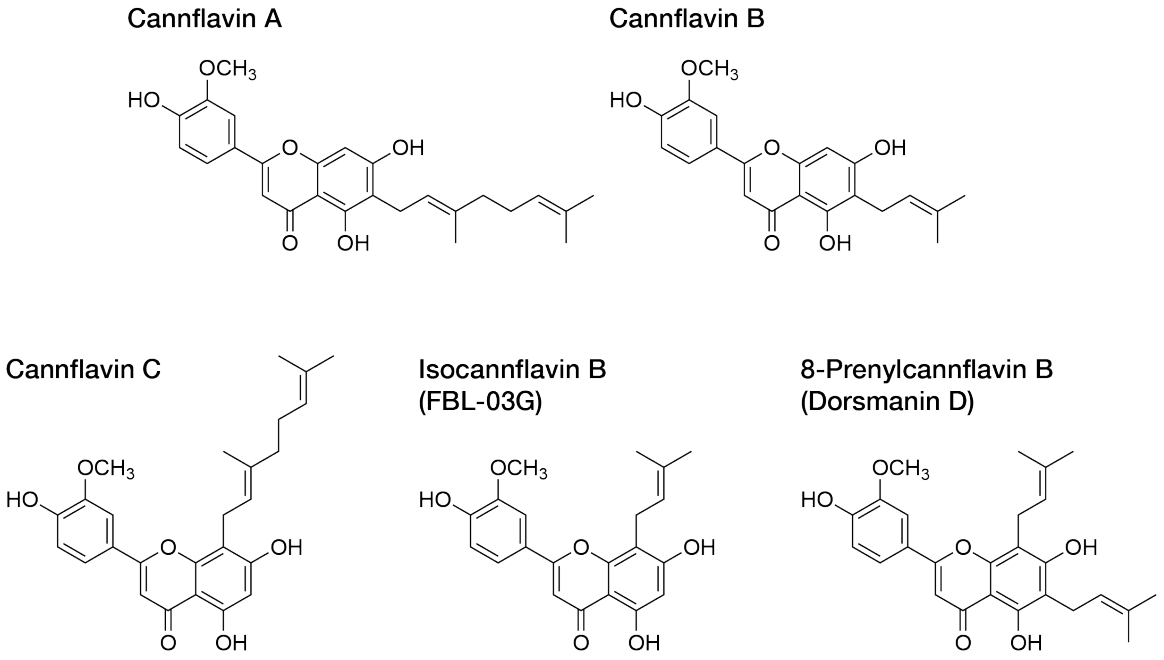

Supplementary Figure 1. Members of the cannflavin family.

SUPPLEMENTARY FIGURE 2

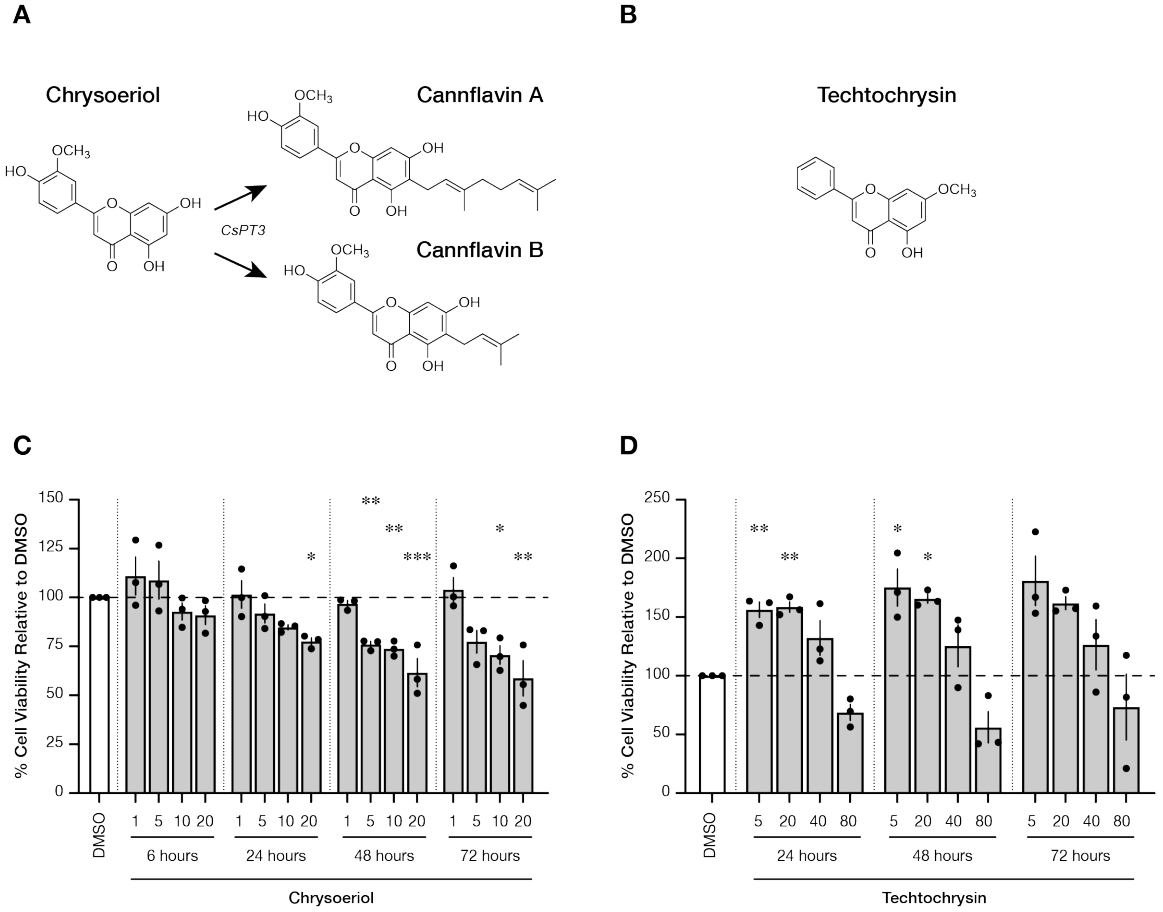

Supplementary Figure 2. Effect of chrysoeriol and techtochrysin on U-87 GBM cell survival. **(A)** Chemical structure of chrysoeriol and **(B)** techtochrysin. As proposed by Real and colleagues (2019), *C. sativa* prenyltransferase 3 (CsPT3) catalyzes the biosynthesis of cannflavins from chrysoeriol. **(C-D)** U-87 cells were treated with increased concentrations of chrysoeriol (1-20 μM) or techtochrysin (5-80 μM), and cell viability was measured at the indicated time-points using the resazurin reduction assay. DMSO was used as a vehicle control. Application of chrysoeriol, but not techtochrysin, reduced the viability of U-87 GBM cells in a dose- and time-dependent manner. A one-way ANOVA was used to analyze the data from each cell line, treatment, and time independently with DMSO as the reference control. Tukey's honestly significant

difference (HSD) post hoc test: * $p < 0.05$, ** $p < 0.01$, *** $p < 0.001$. Graphs represent mean ± SEM ($n = 3$).

SUPPLEMENTARY FIGURE 3

A A-172 LDH Release Assay (24 h)

	% LDH release	SEM
Lysis buffer		
Positive control	100	–
Vehicle (DMSO)		
Negative control	1.77	0.65
Cannflavin A		
10 μM	3.57	0.84
20 μM	2.54	0.66
Cannflavin B		
10 μM	4.43	1.43
20 μM	5.38	1.44
ANA-12		
10 μM	2.01	0.48
50 μM	11.35	3.63

B U-87 LDH Release Assay (24 h)

	% LDH release	SEM
Lysis buffer		
Positive control	100	–
Vehicle (DMSO)		
Negative control	1.57	0.29
Cannflavin A		
10 μM	0.96	0.09
20 μM	1.03	0.08
Cannflavin B		
10 μM	0.81	0.05
20 μM	0.88	0.07
ANA-12		
10 μM	1.61	0.26
50 μM	10.71	0.64

C

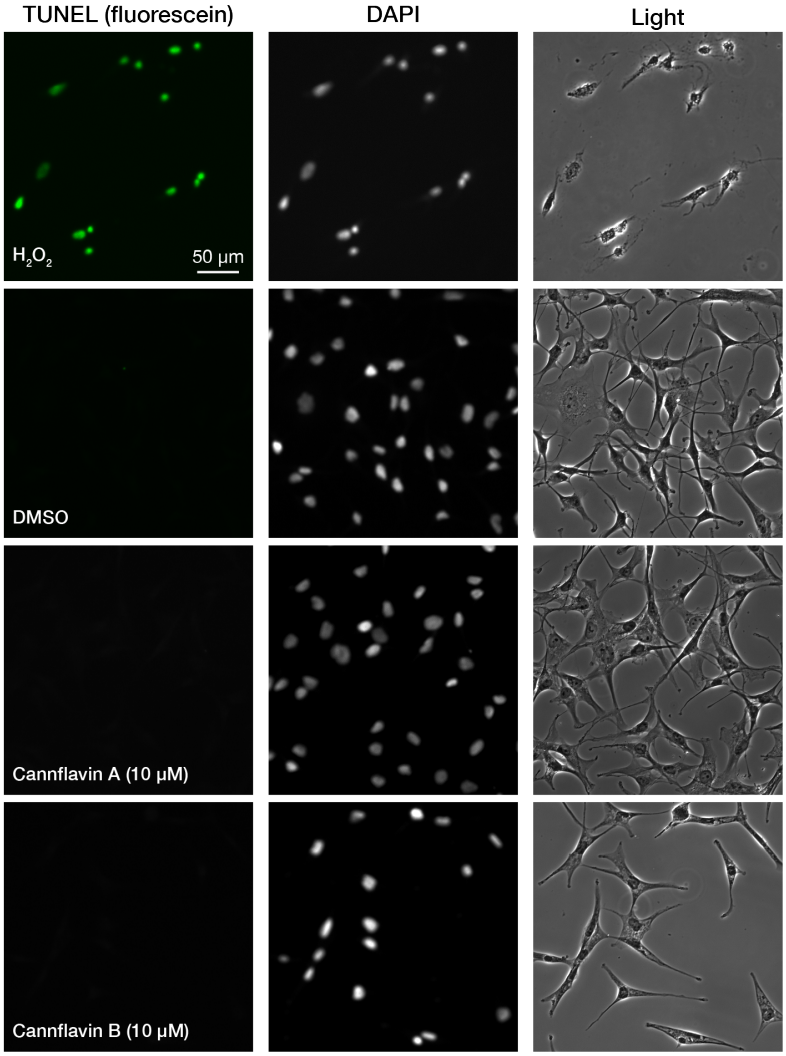

Supplementary Figure 3. Effects of cannflavins A and B on LDH release and DNA fragmentation. **(A)** A-172 and **(B)** U-87 GBM cells were treated with cannflavin A or cannflavin B at 10 and 20 μM final concentrations, or ANA-12 (10 and 50 μM final concentration), and percent LDH release into cell culture media was quantified using the Invitrogen CyQUANT LDH Cytotoxicity Assay Kit. **(C)** Representative immunofluorescent images of A-172 GBM cells after 24 hours of treatment with cannflavins (10 μM final concentration) probed using TUNEL (fluorescein, green signal represent the occurrence of double-stranded DNA breaks). Nuclei were stained with DAPI (middle panels). Hydrogen peroxide (H_2O_2) was used as a positive control (applied directly to cell culture media for 10 minutes at a final concentration of 100 μM), and DMSO as the vehicle control for cannflavins. Scale bar = 50 μm.

SUPPLEMENTARY VIDEO 1

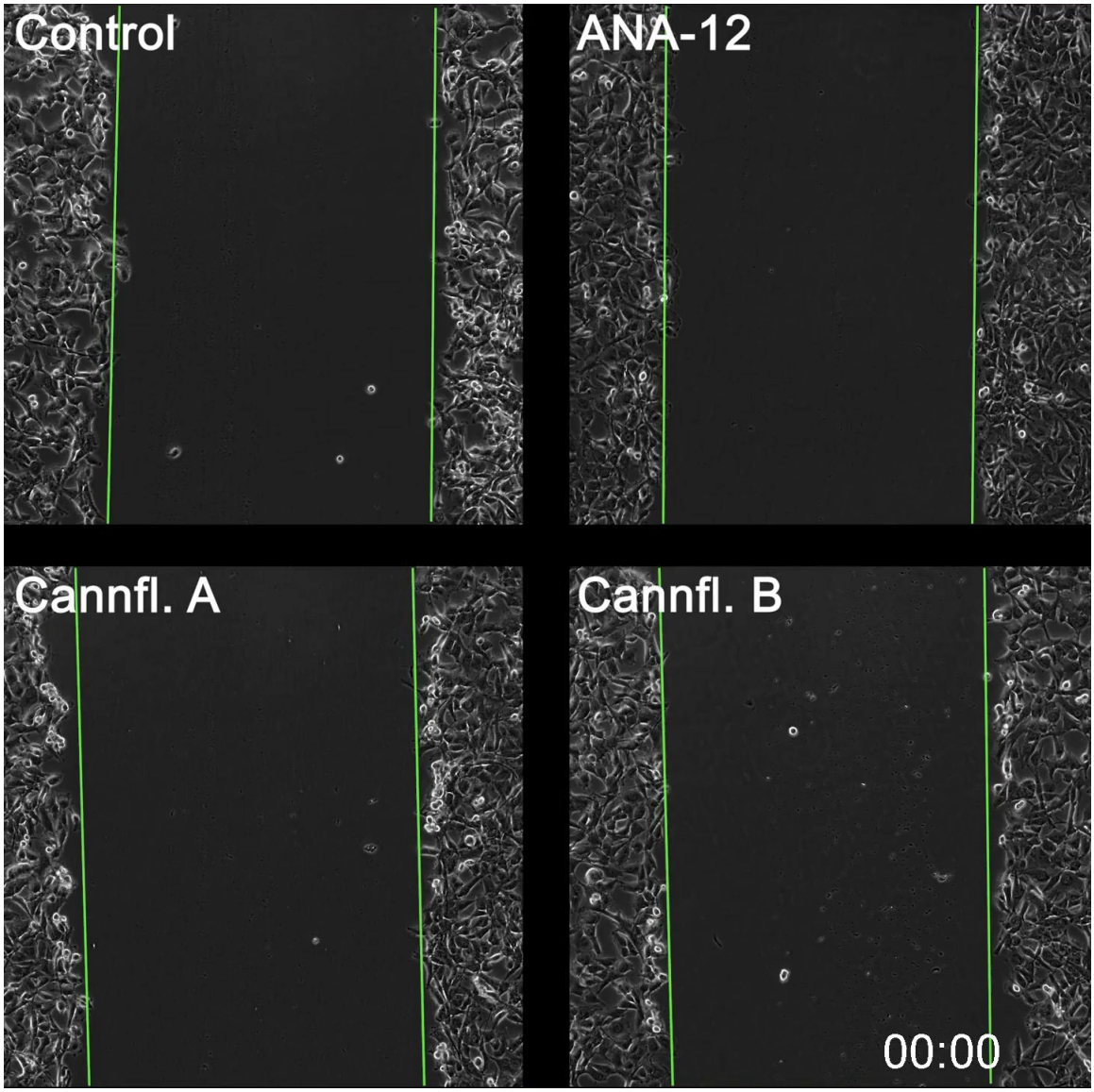

Supplementary Video 1. Scratch migration assay video. The green lines represent the initial boundaries ($t = 0$) of the scratched wound.